

**PIERRE
AUGER**
OBSERVATORY

Latest results from the Pierre Auger Observatory

(cosmic rays, the Auger detectors, observations)

Jose Bellido

(On behalf of the Pierre Auger Collaboration)

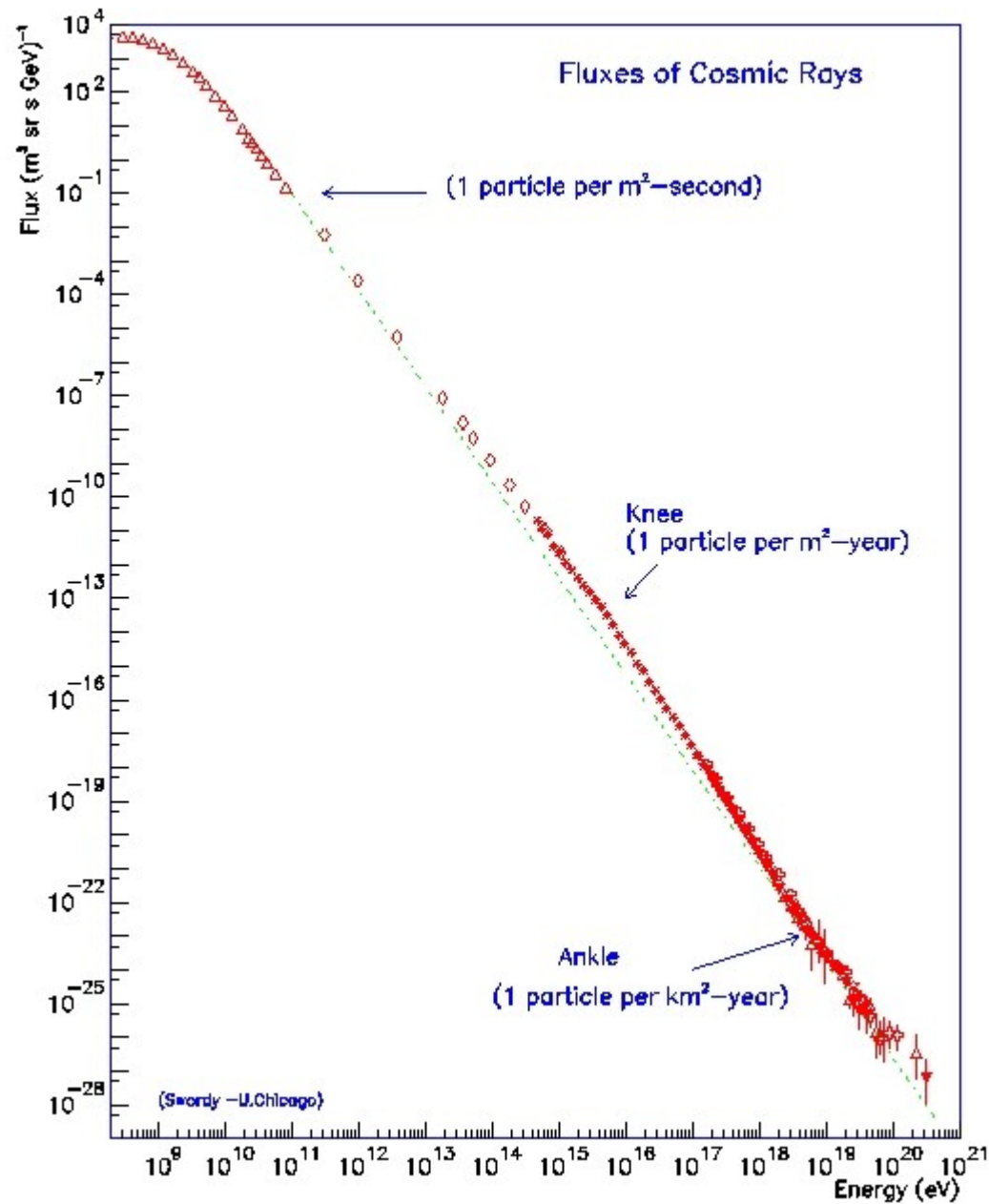


THE UNIVERSITY
of ADELAIDE

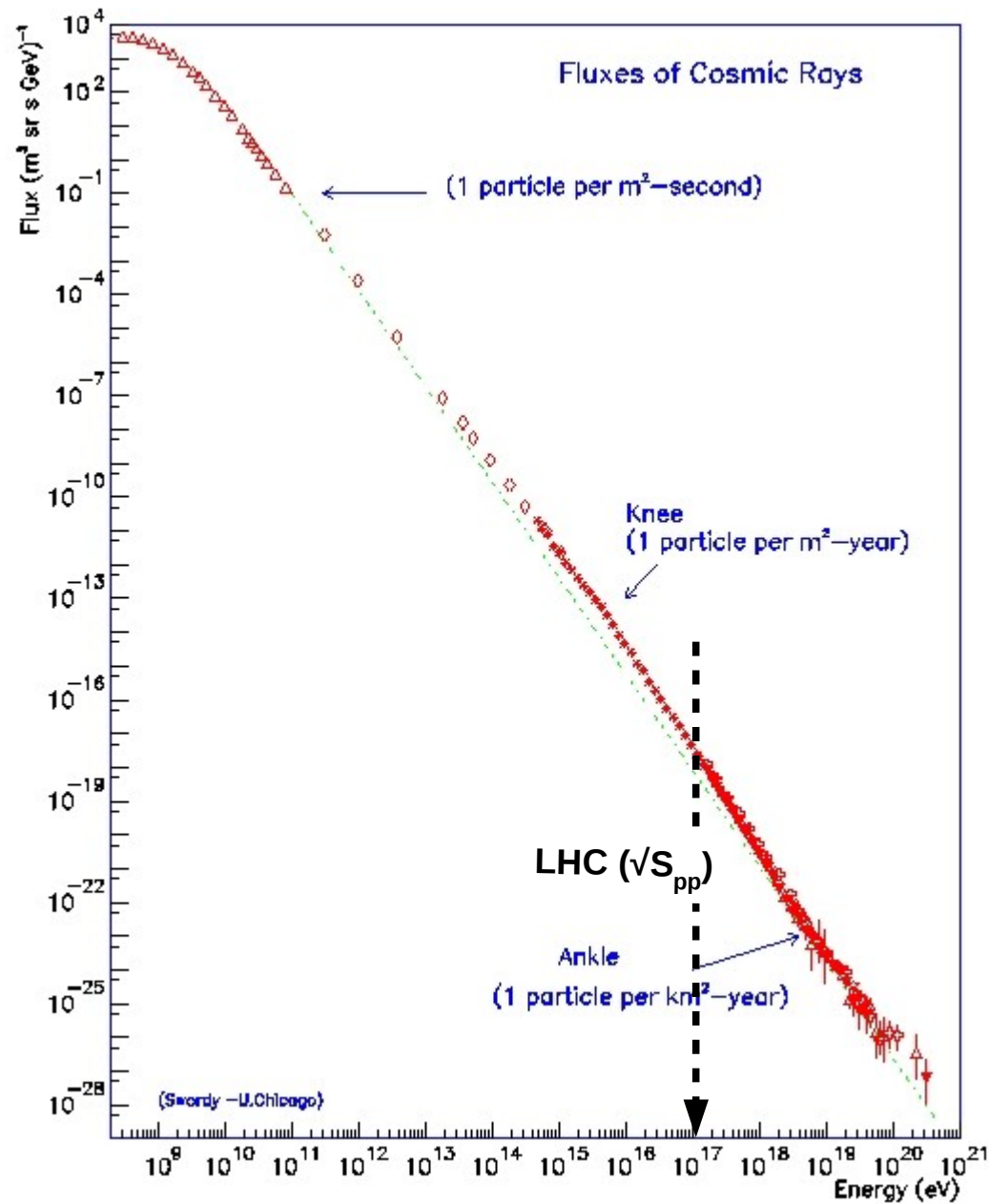
13th International Symposium on Cosmology and Particle Astrophysics (CosPA 2016)

Sydney, November 29th 2016

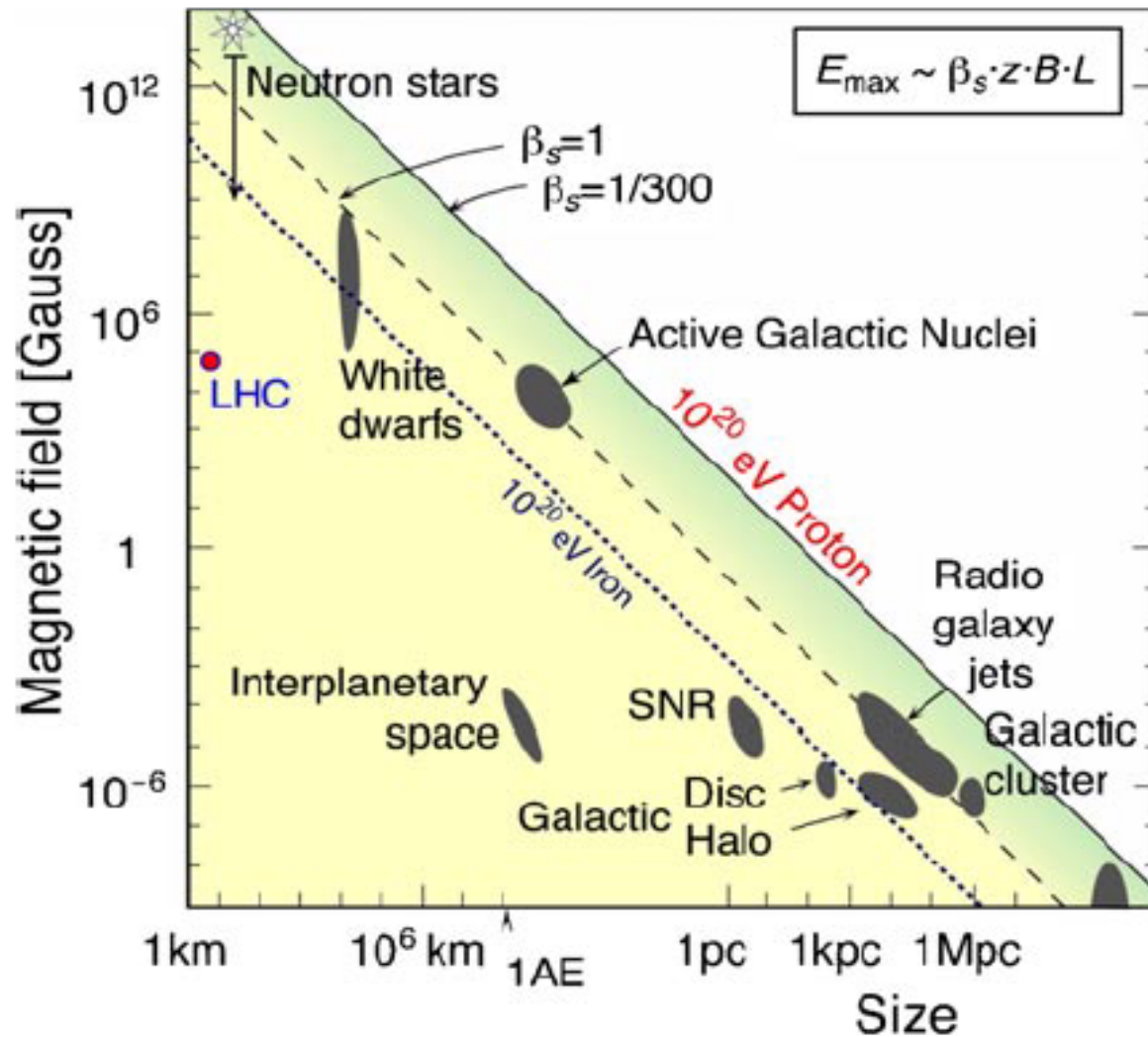
Cosmic Rays flux as a function of energy



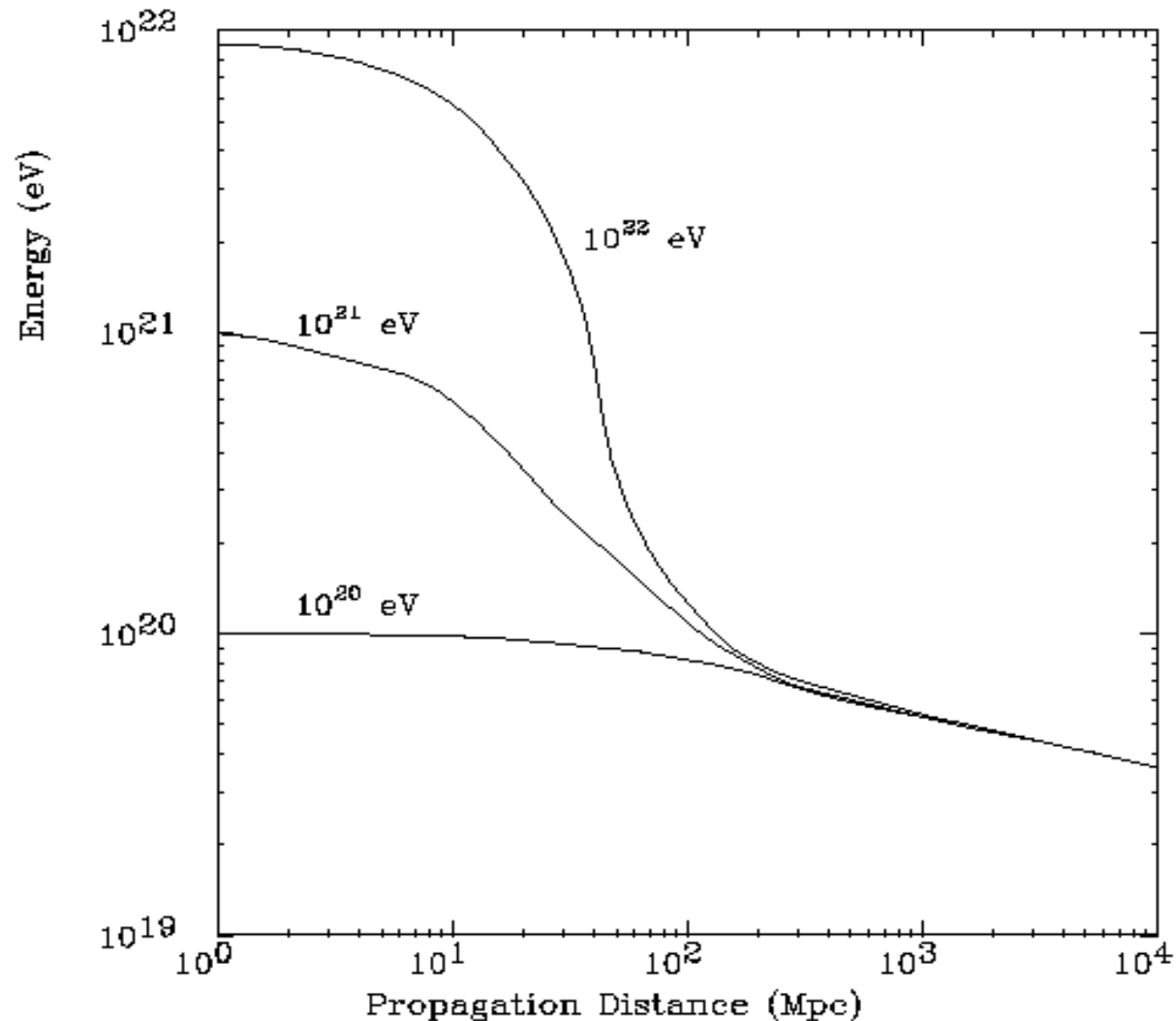
Cosmic Rays flux as a function of energy



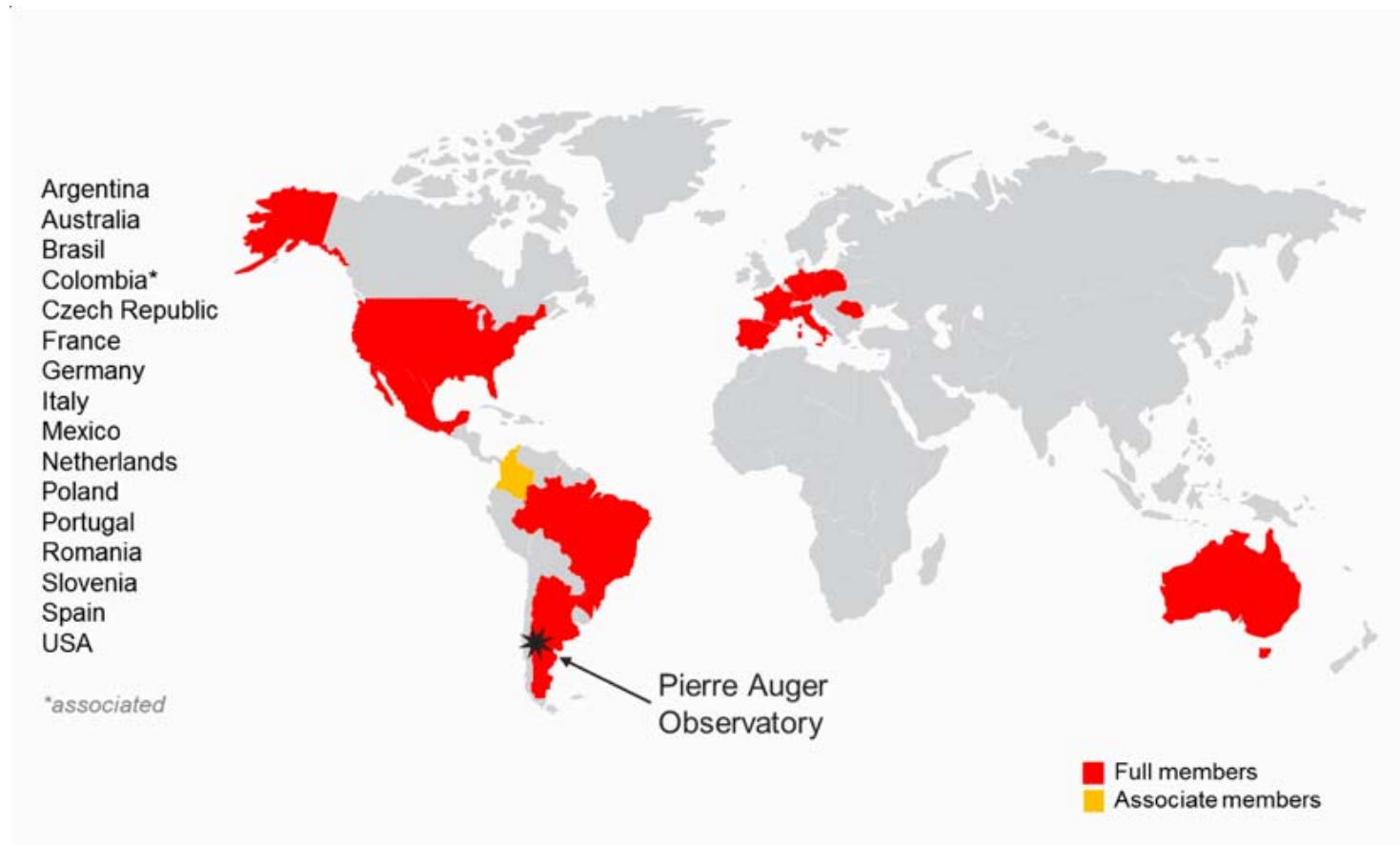
There is not clear explanation for cosmic rays with energies above 10^{20} eV

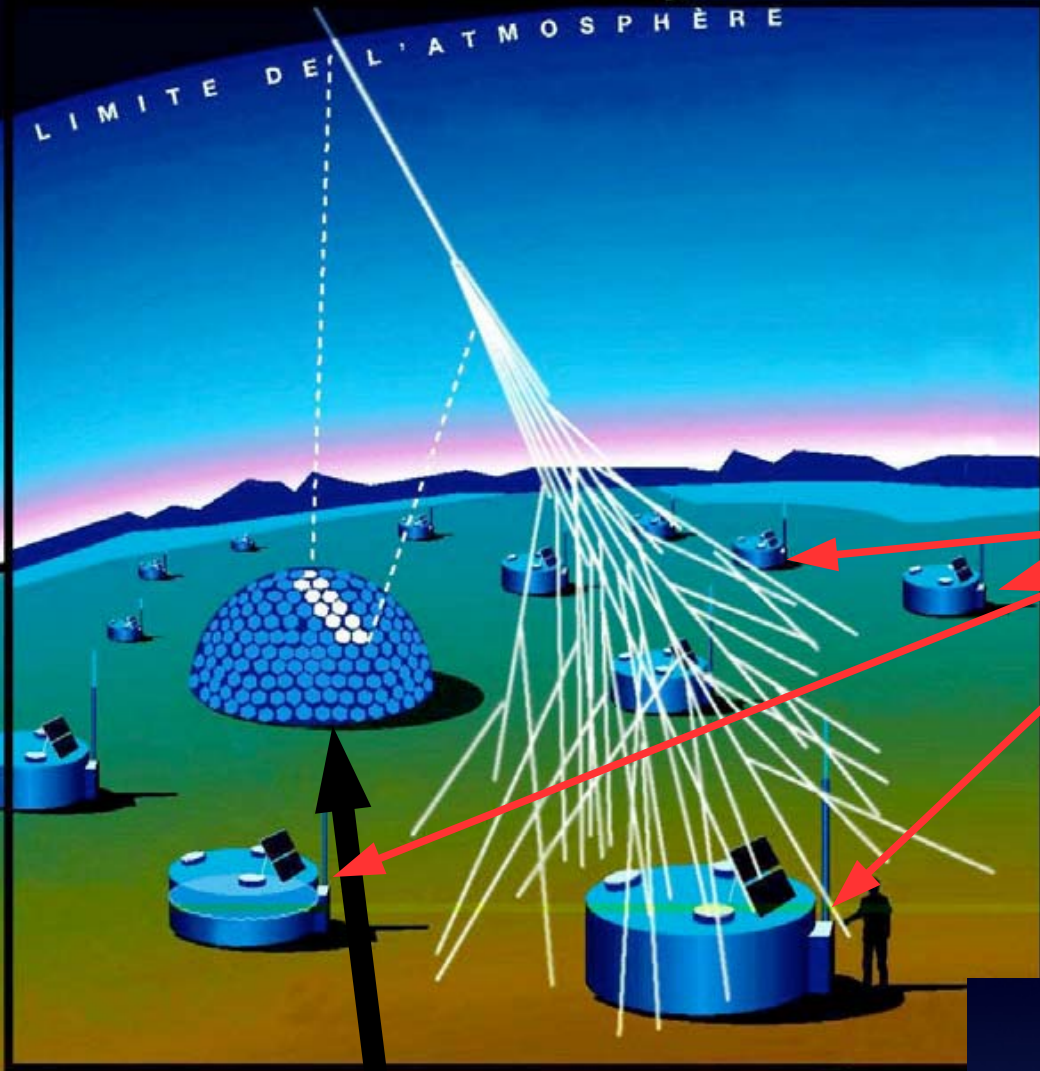


Protons with energies above 6×10^{19} eV interact with the microwave background radiation (CMB) and they rapidly lose energy (GZK cutoff)



The Pierre Auger Collaboration

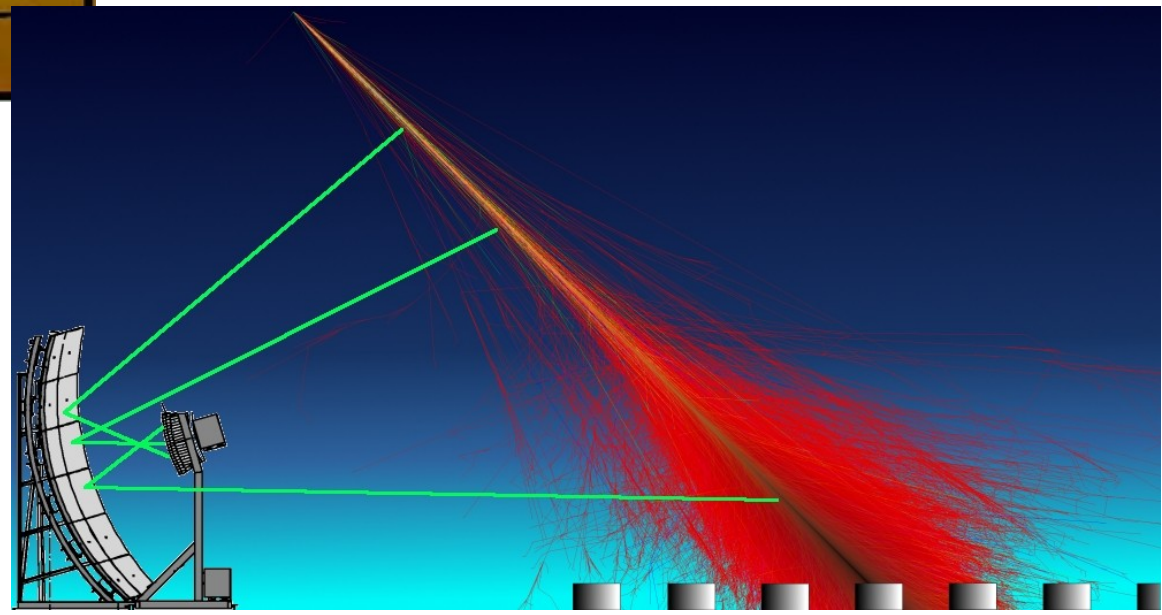




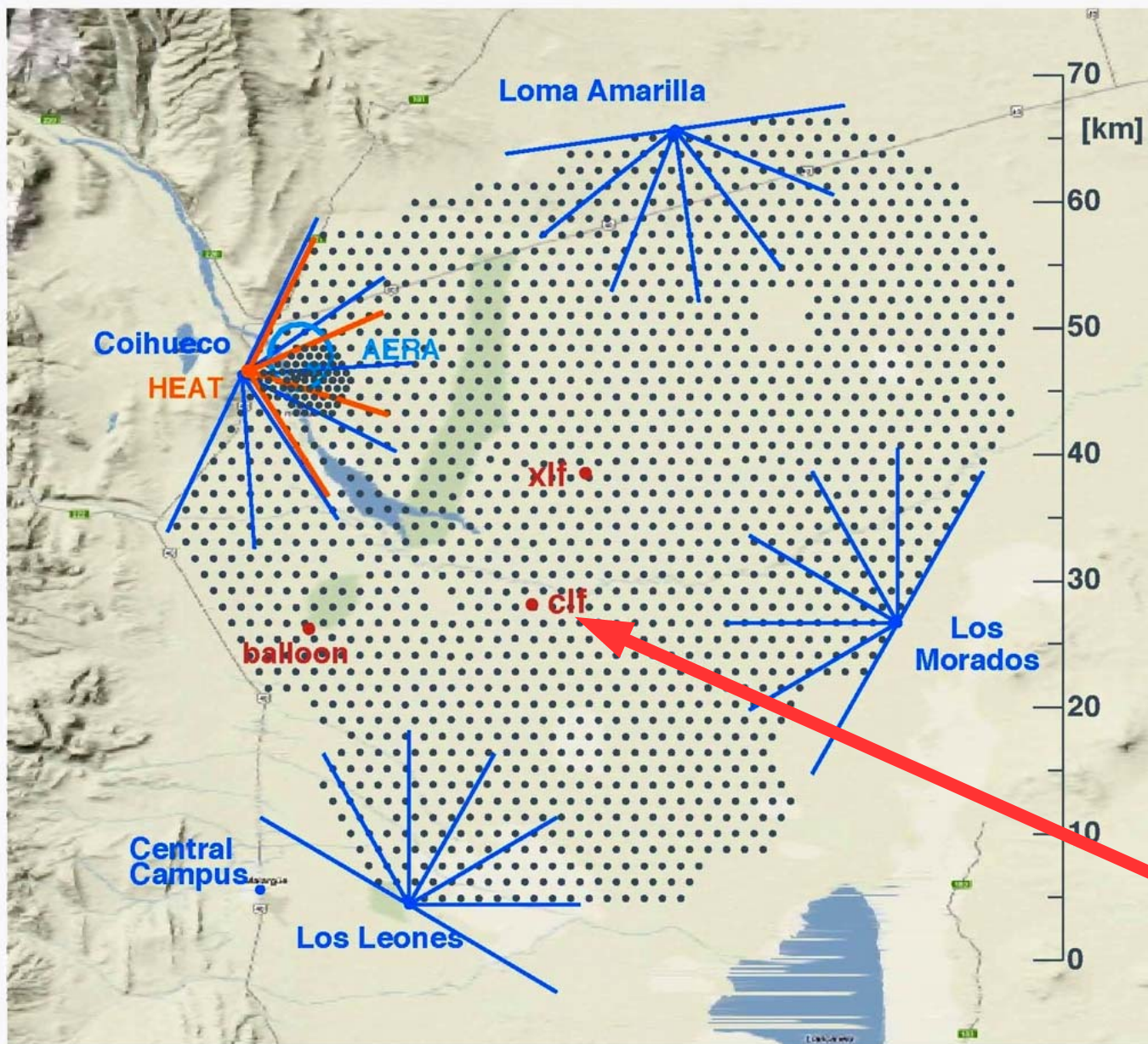
“The Pierre Auger Observatory...employing a giant array of particle counters and an optical fluorescence detector...is a “hybrid” ground detector...”

Surface Detector (SD)

Fluorescence Detector (FD)



The Pierre Auger Observatory, Argentina



SD station (1500 stations)



FD (4 sites + HEAT)



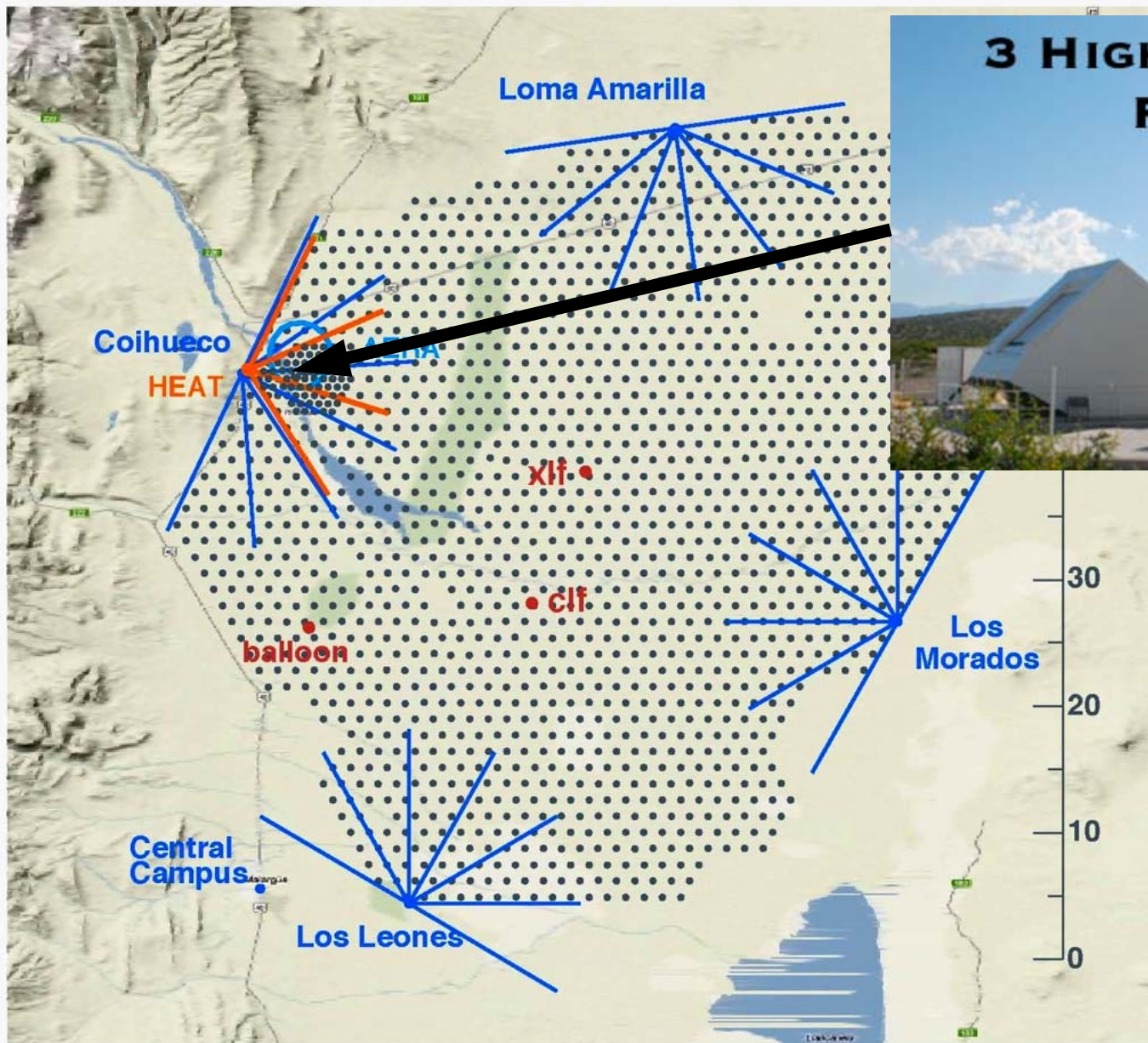
Laser station (CLF)

For monitoring: atmosphere, timing, FD alignment, and reconstruction performance



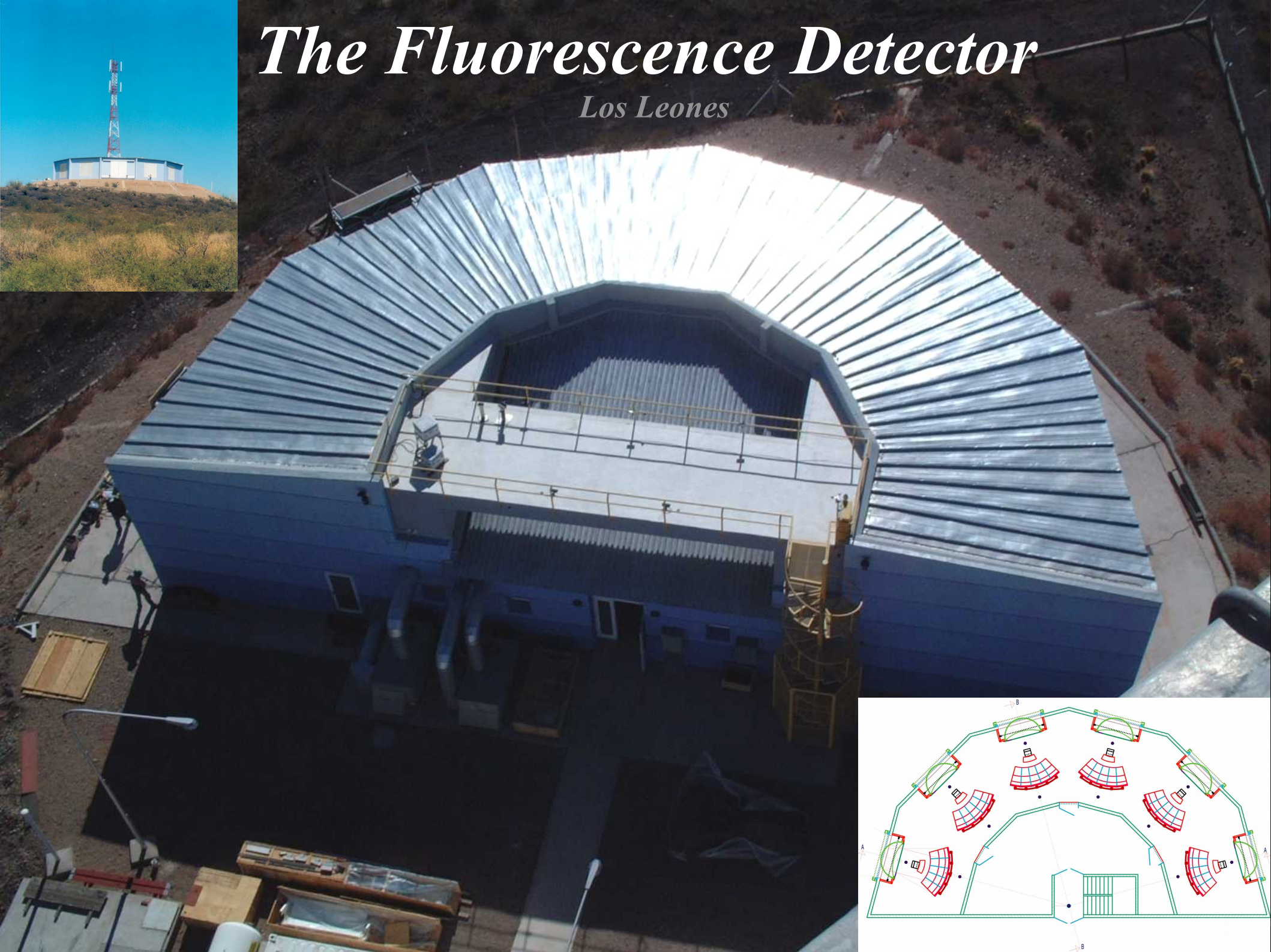
The Pierre Auger Observatory, Argentina

HEAT

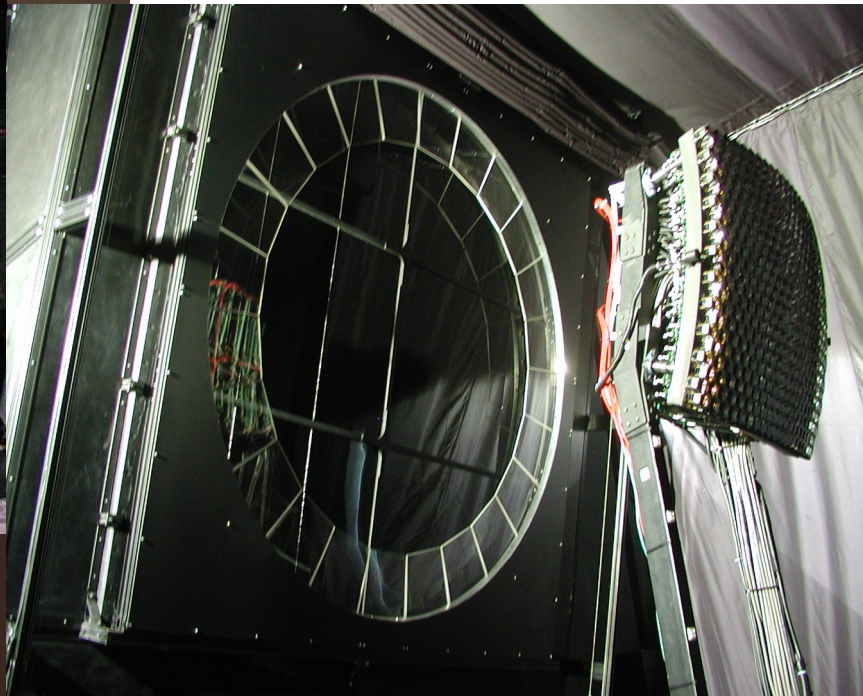
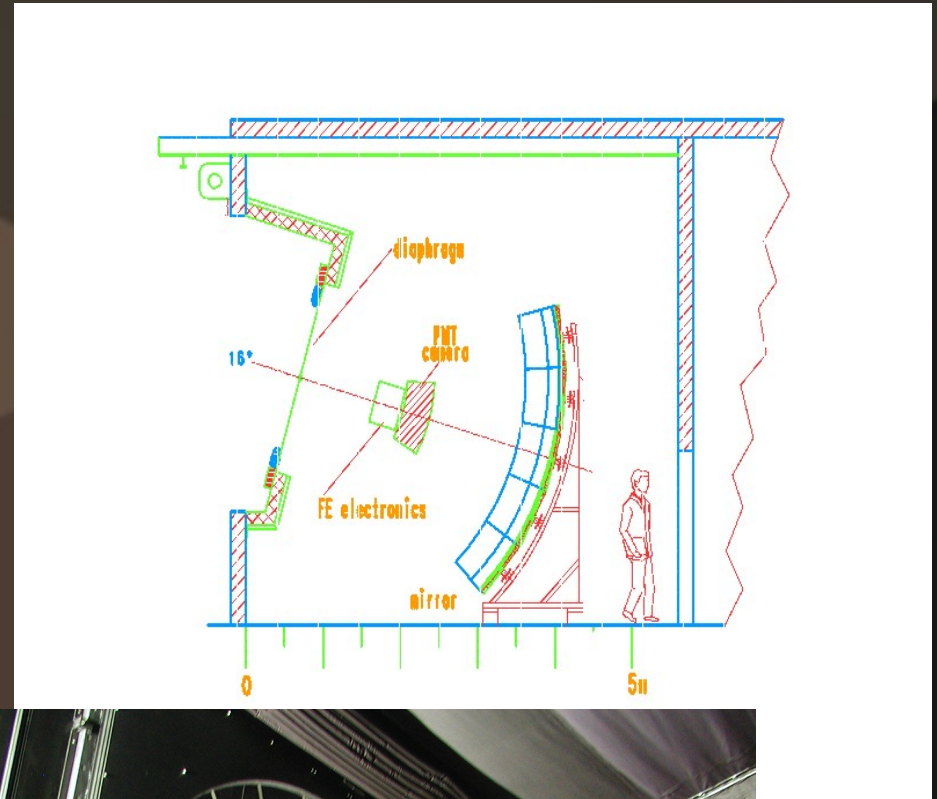
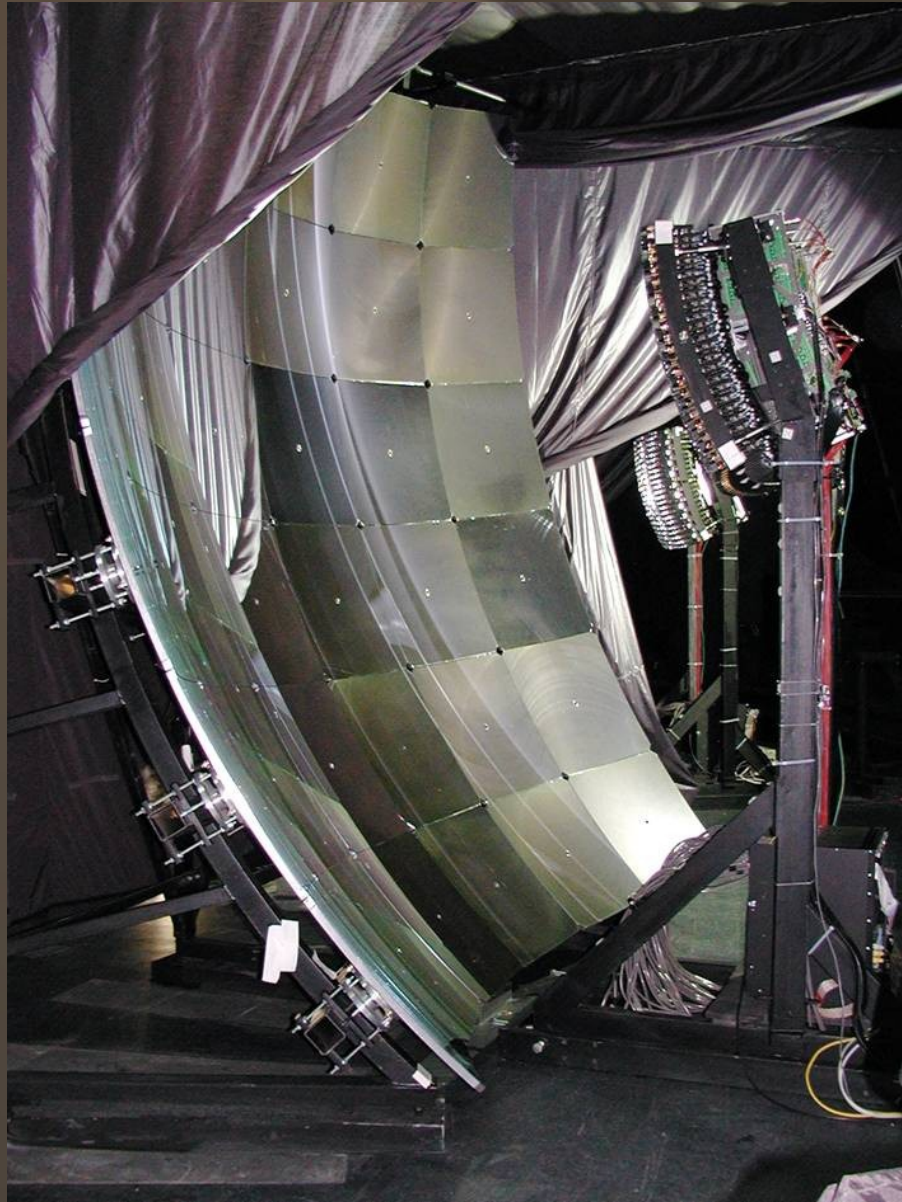


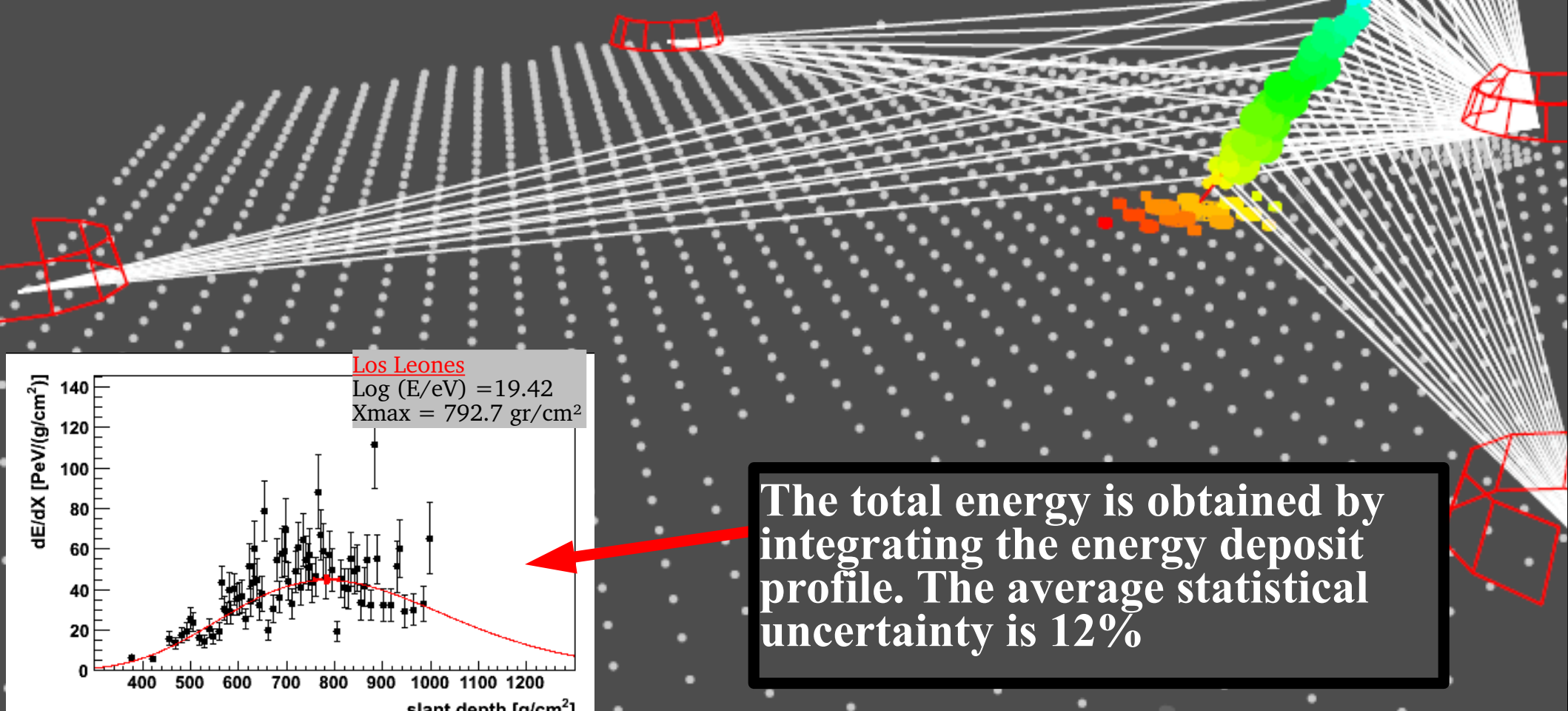
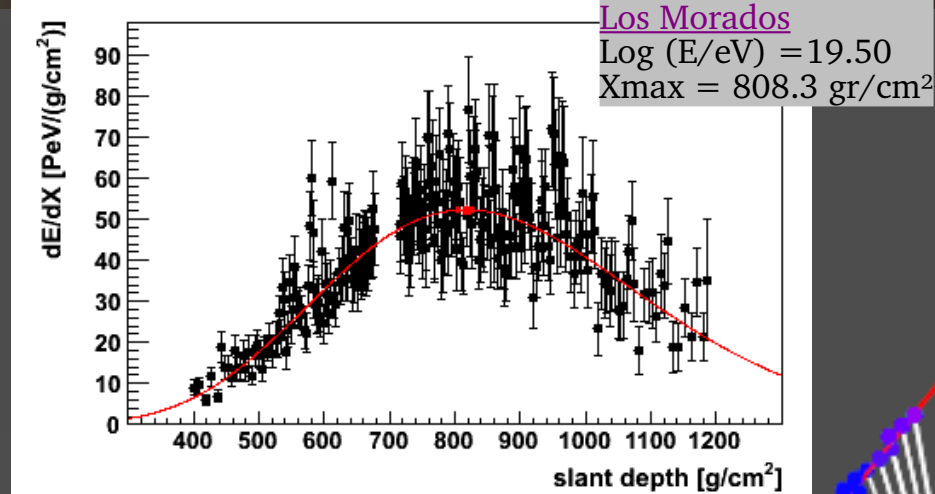
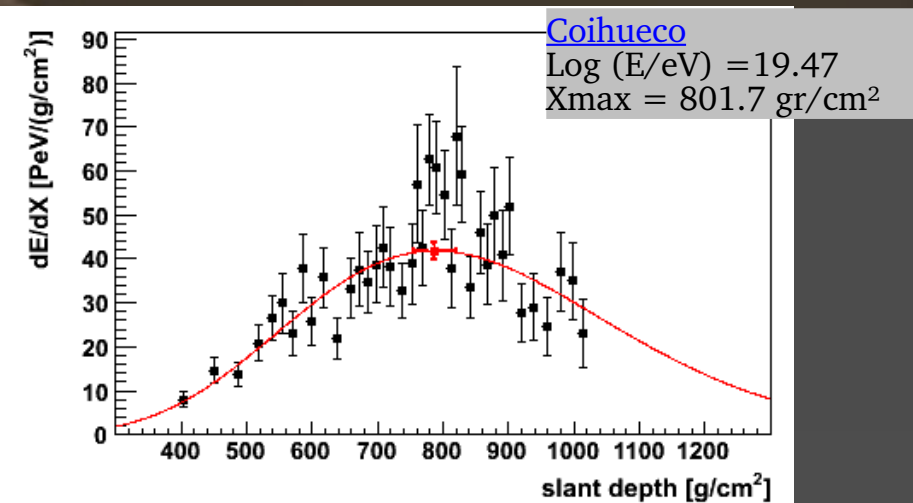
The Fluorescence Detector

Los Leones



The Fluorescence Detector





The total energy is obtained by integrating the energy deposit profile. The average statistical uncertainty is 12%

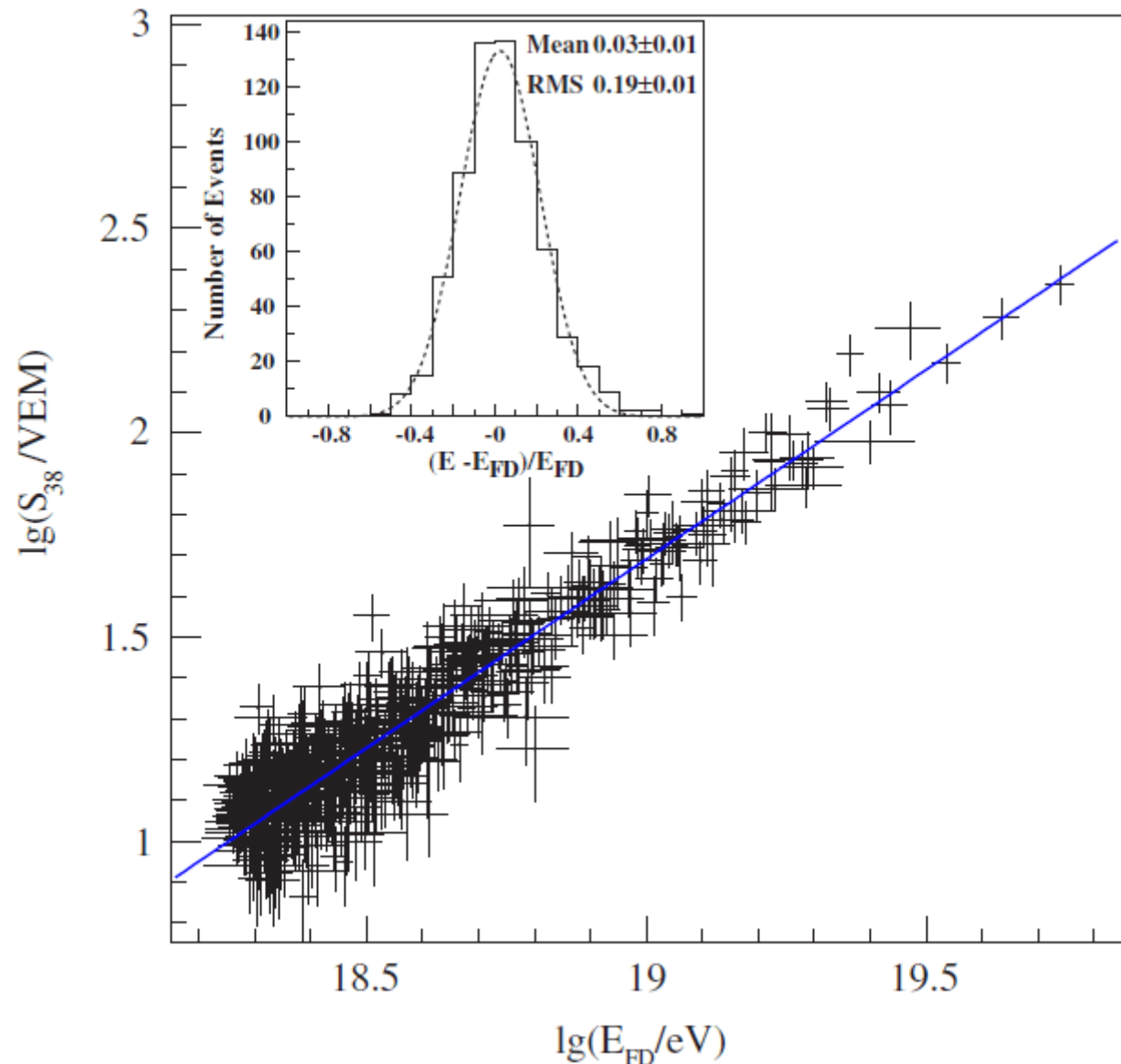
The Energy scale from the FD is transferred to the SD

The energy converter:

Compare ground parameter $S(1000)$ with the fluorescence detector energy.

The **systematic uncertainties** of the fluorescence detector (14%) are transferred to the surface detector.

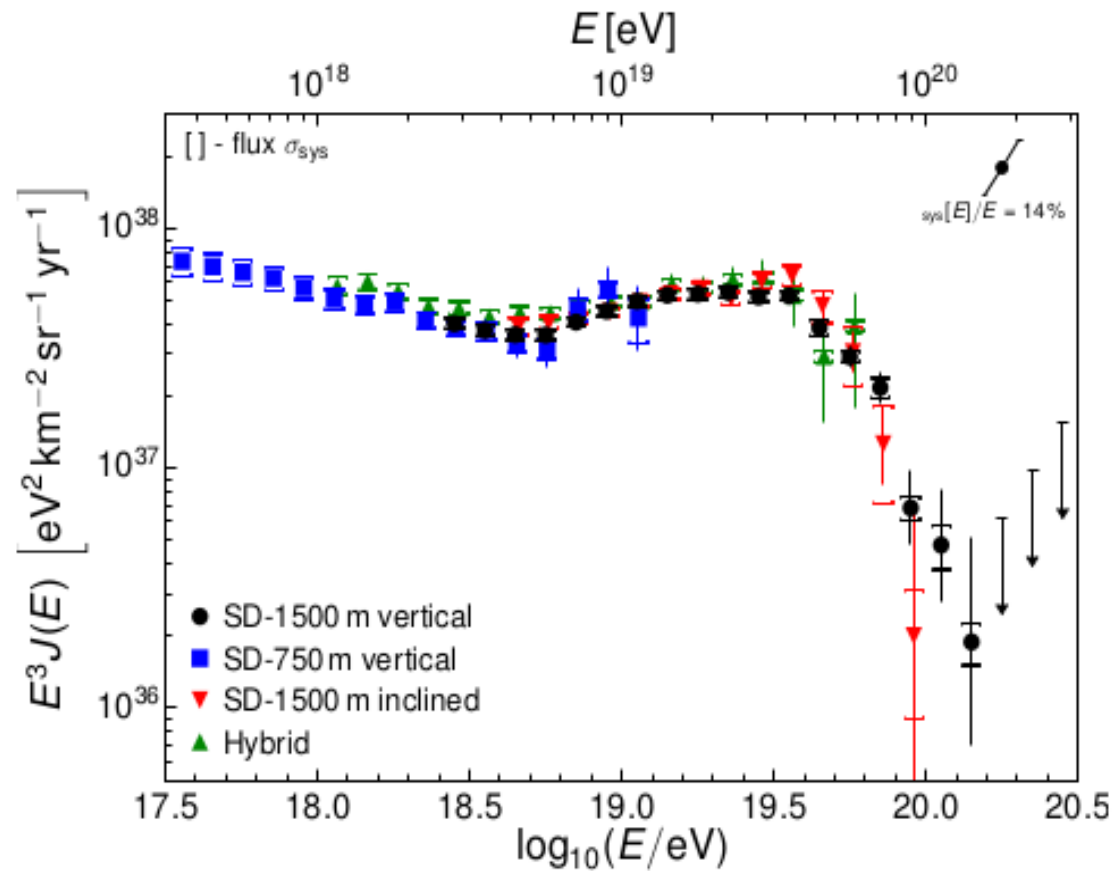
The surface detector **energy resolution** is about 20% at the lowest energies and 10% at the highest energies.



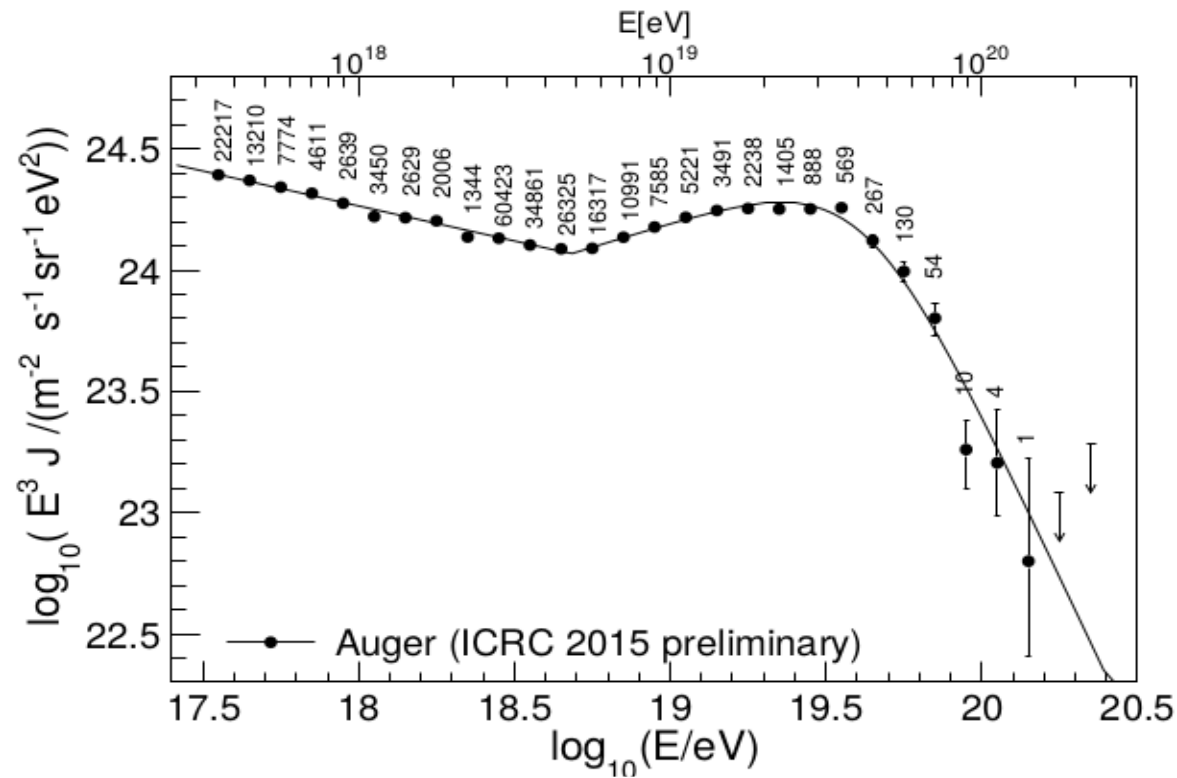
Note: S_{1000} for a given shower energy varies depending on the zenith angle. So, S_{38} is the corresponding expectation for a 38° shower, given the S_{1000} measurement.

The Cosmic Ray Energy Spectrum

Four independent measurements



The Cosmic Ray Energy Spectrum (combining all measurements)



Fitted function:

$$J(E) = J_0 \left(\frac{E}{E_{\text{ankle}}} \right)^{-\gamma_1}$$

$$E < E_{\text{ankle}}$$

$$J(E) = J_0 \left(\frac{E}{E_{\text{ankle}}} \right)^{-\gamma_2} \left[1 + \left(\frac{E_{\text{ankle}}}{E_s} \right)^{\Delta\gamma} \right] \left[1 + \left(\frac{E}{E_s} \right)^{\Delta\gamma} \right]^{-1}$$

$$E > E_{\text{ankle}}$$

Fitted parameters:

J_0 [$\text{eV}^{-1}\text{km}^{-2}\text{sr}^{-1}\text{yr}^{-1}$]	E_{ankle} [EeV]	E_s [EeV]	γ_1	γ_2	$\Delta\gamma$
$(3.30 \pm 0.15 \pm 0.20) \times 10^{-19}$	$4.82 \pm 0.07 \pm 0.8$	$42.09 \pm 1.7 \pm 7.61$	$3.29 \pm 0.02 \pm 0.05$	$2.60 \pm 0.02 \pm 0.1$	$3.14 \pm 0.2 \pm 0.4$

Arrival Directions

Cross correlation studies

Objects	E_{th} [EeV]	Ψ [°]	D [Mpc]	\mathcal{L}_{min} [erg/s]	f_{min}	\mathcal{P}
2MRS Galaxies	52	9	90	-	1.5×10^{-3}	24%
Swift AGNs	58	1	80	-	6×10^{-5}	6%
Radio galaxies	72	4.75	90	-	2×10^{-4}	8%
Swift AGNs	58	18	130	10^{44}	2×10^{-6}	1.3%
Radio galaxies	72	4.75	90	$10^{39.33}$	5.1×10^{-5}	11%
Centaurus A	58	15	-	-	2×10^{-4}	1.4%

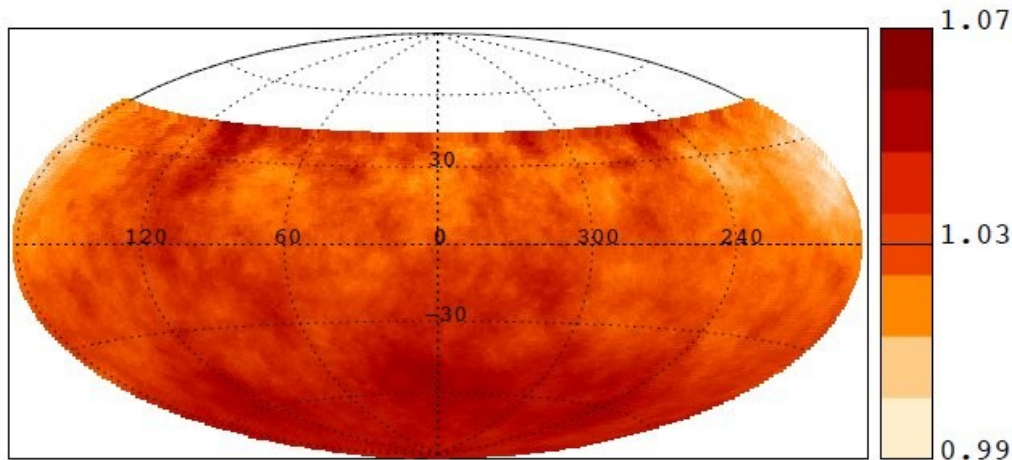
Table 1: Summary of the parameters of the minima found in the cross-correlation analyses.

THE ASTROPHYSICAL JOURNAL, 804:15 (18pp), 2015

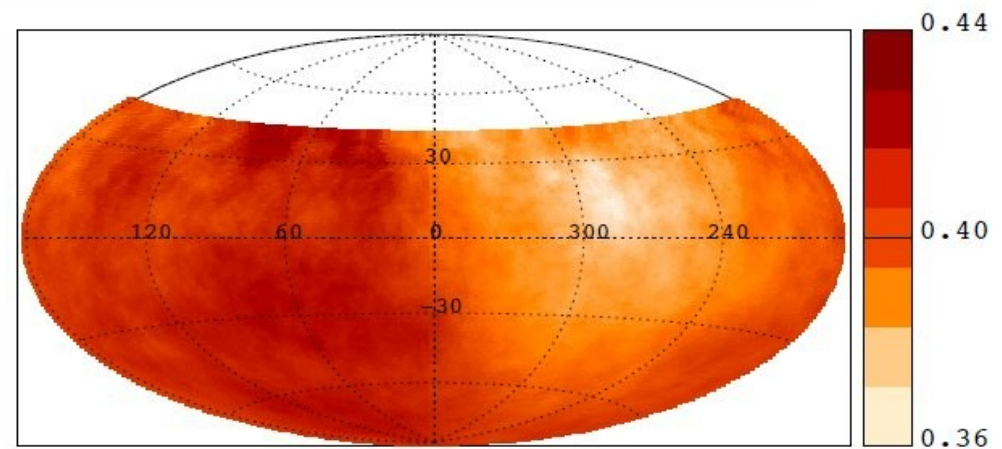
Harmonic analysis in right ascension
85% sky coverage

Sky map of the CR flux (45° smoothing)

4 EeV < E < 8 EeV

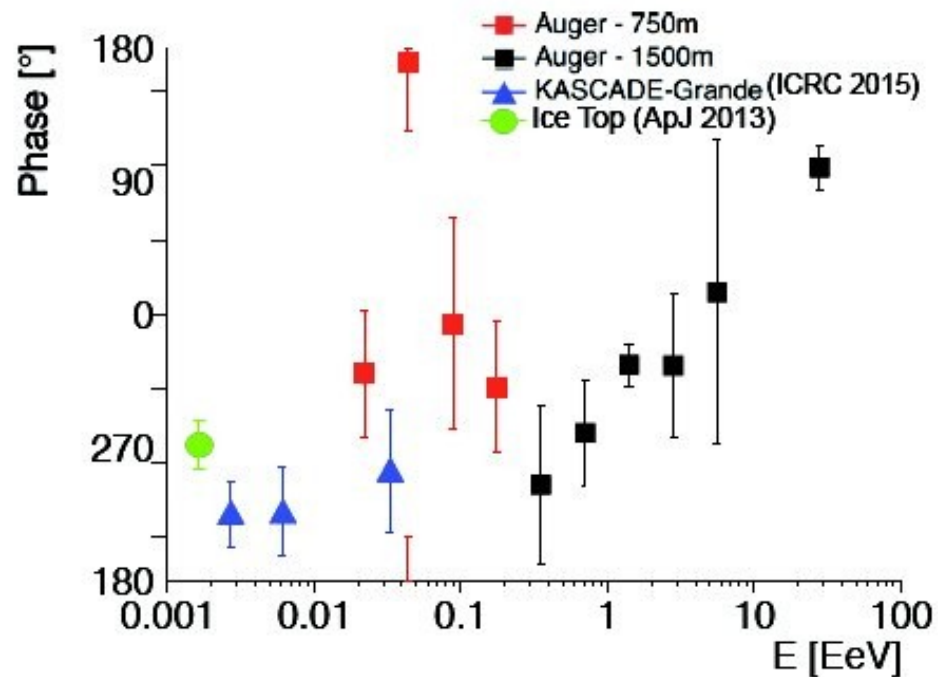


E > 8 EeV

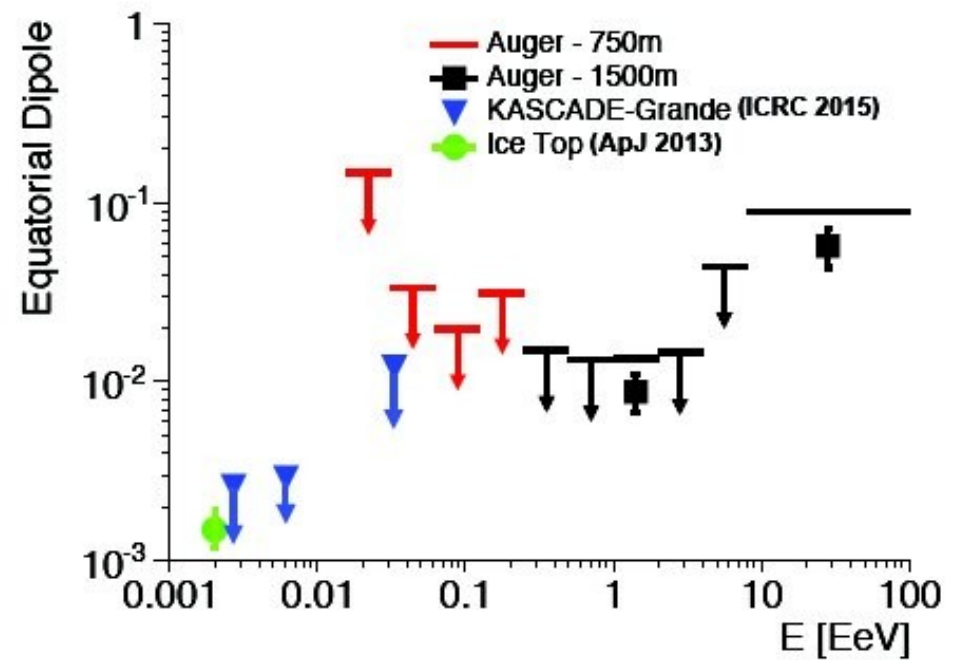


Dipole amplitude: $7.3 \pm 1.5\%$ ($p=6.4 \times 10^{-5}$)
Pointing to $(a,d) = (95^\circ \pm 13^\circ, 39^\circ \pm 13^\circ)$

DIPOLE PHASE



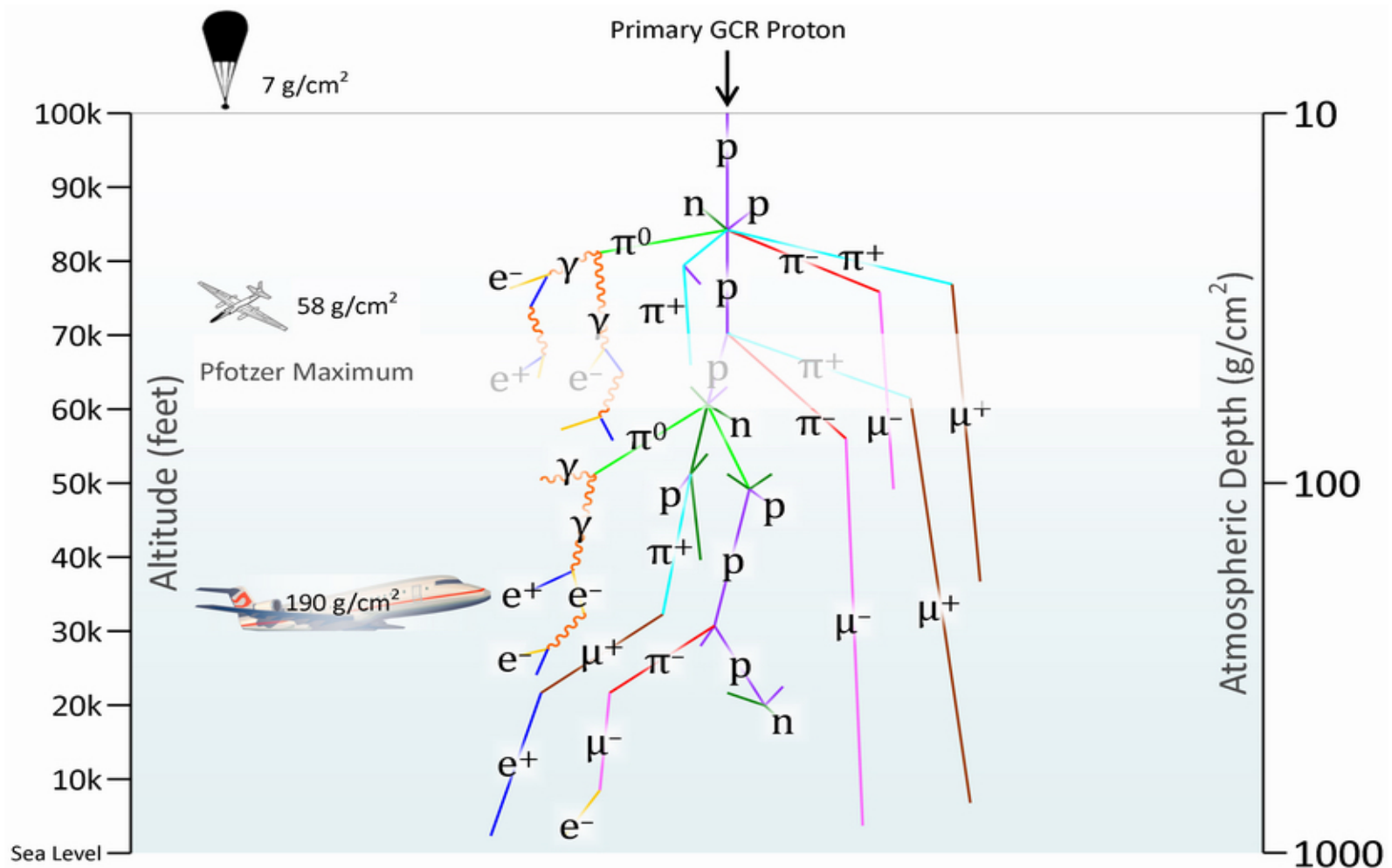
DIPOLE AMPLITUDE



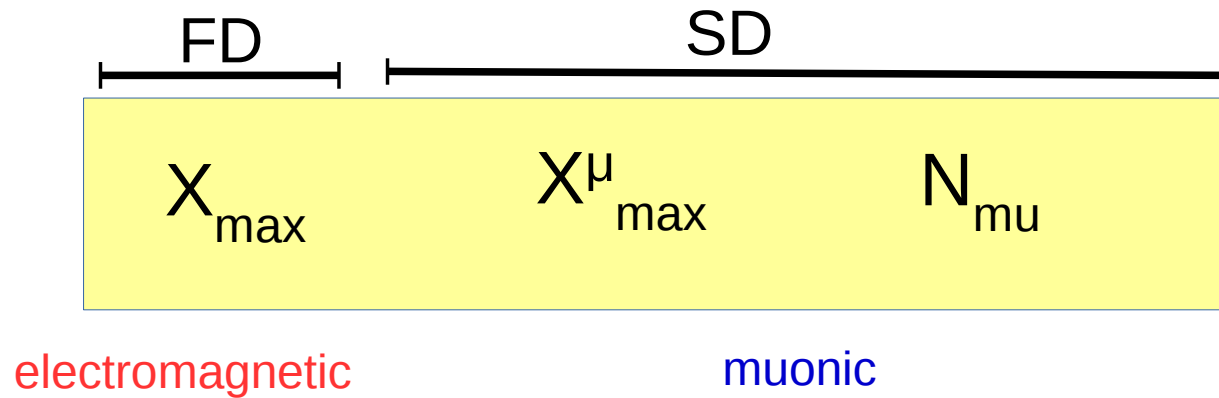
Evolution of an Air Shower

An air shower has three main components:

- a) the **electromagnetic**
- b) the **muonic**, and
- c) the hadronic.



Auger measurements related to mass composition

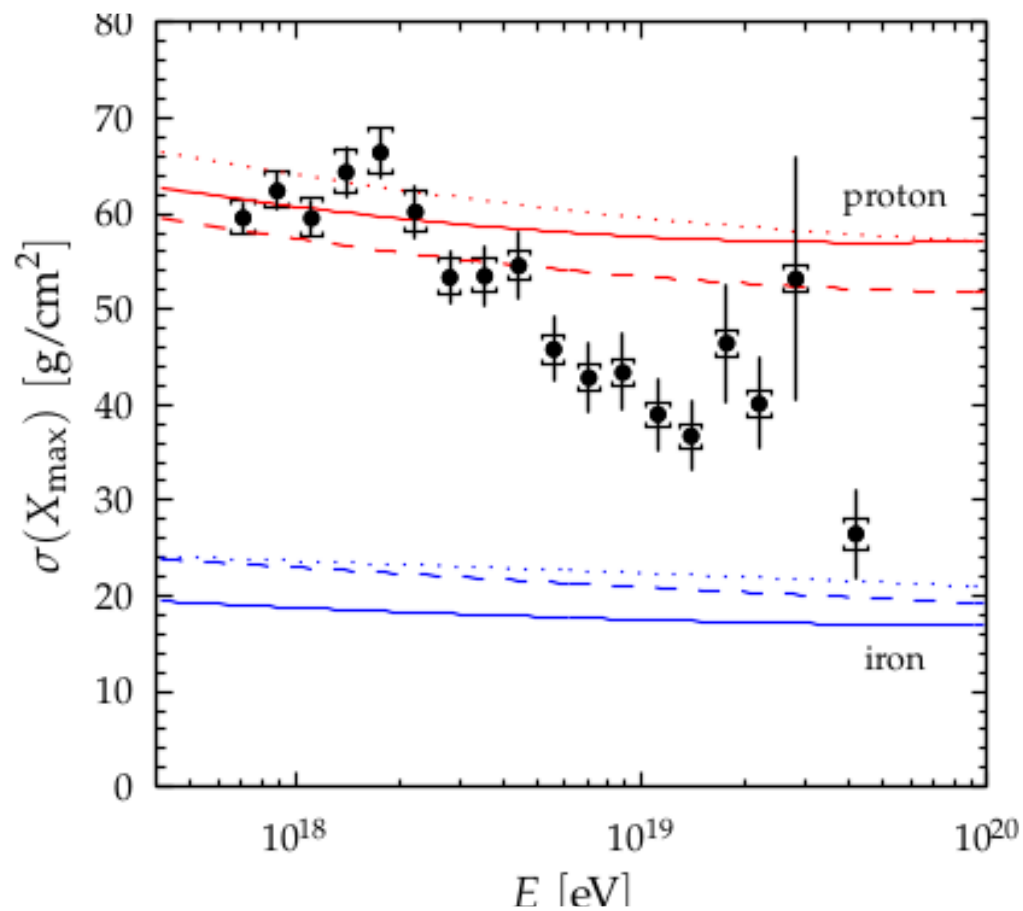
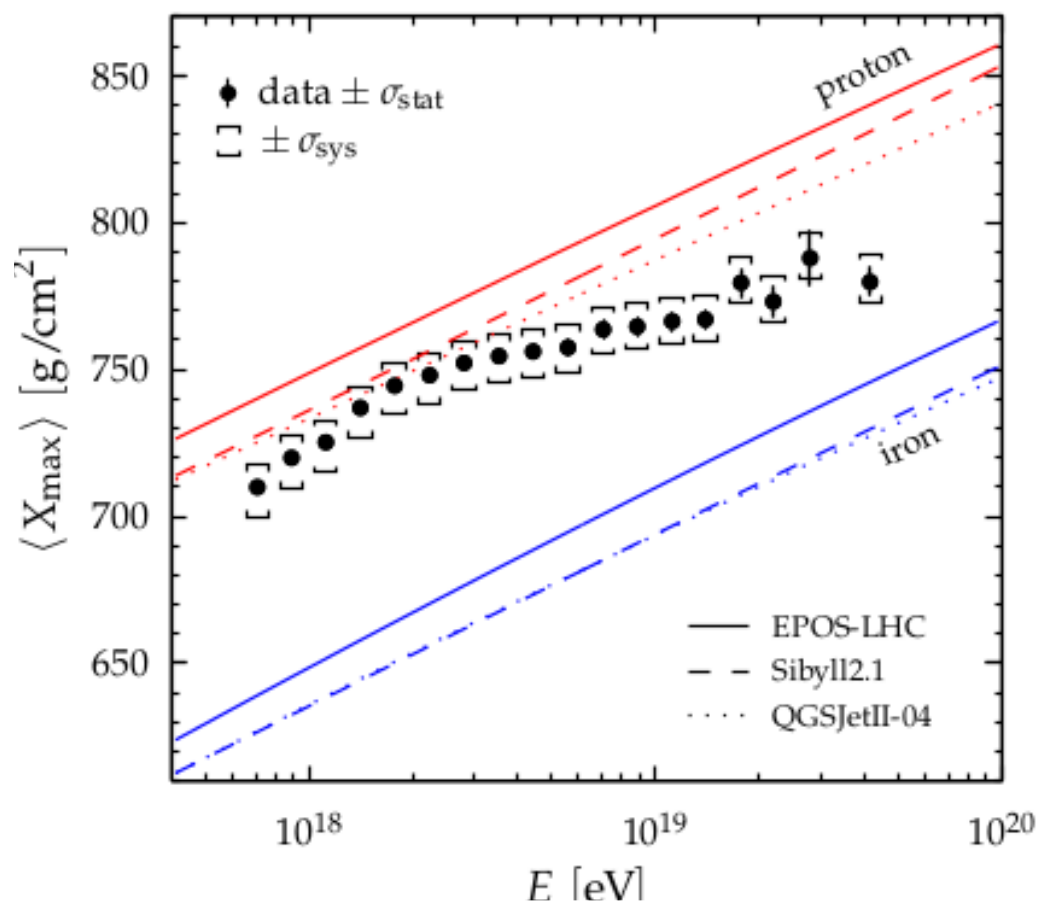


Correlation factor between:

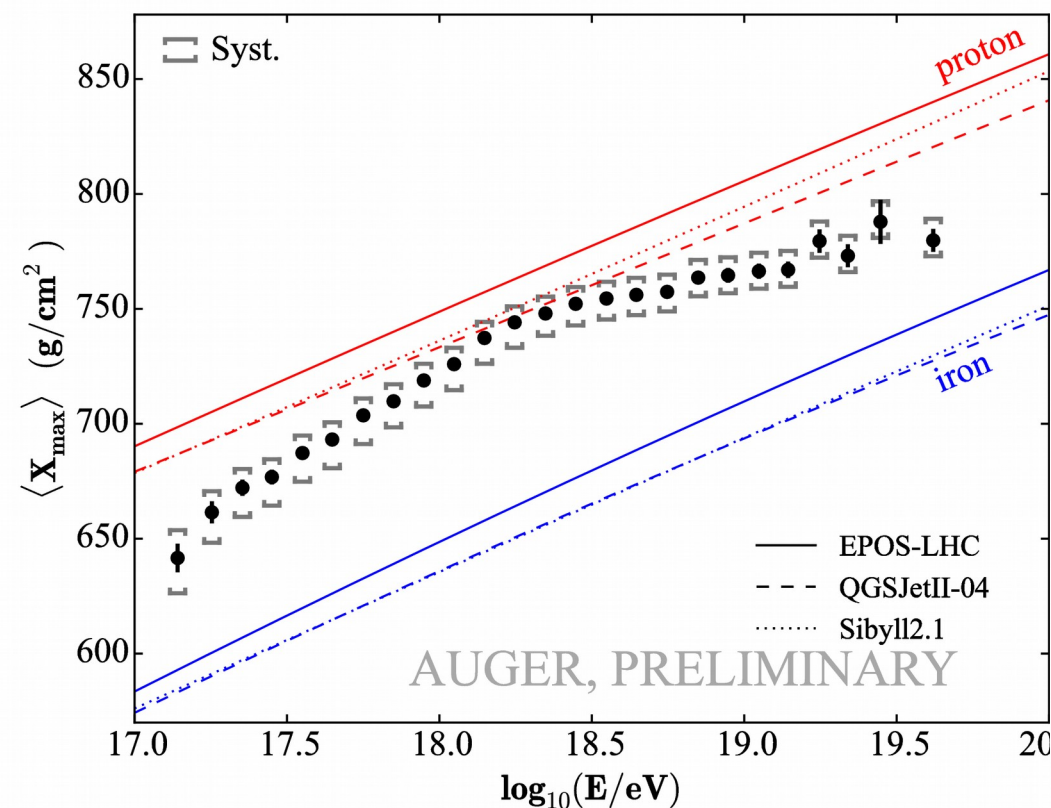
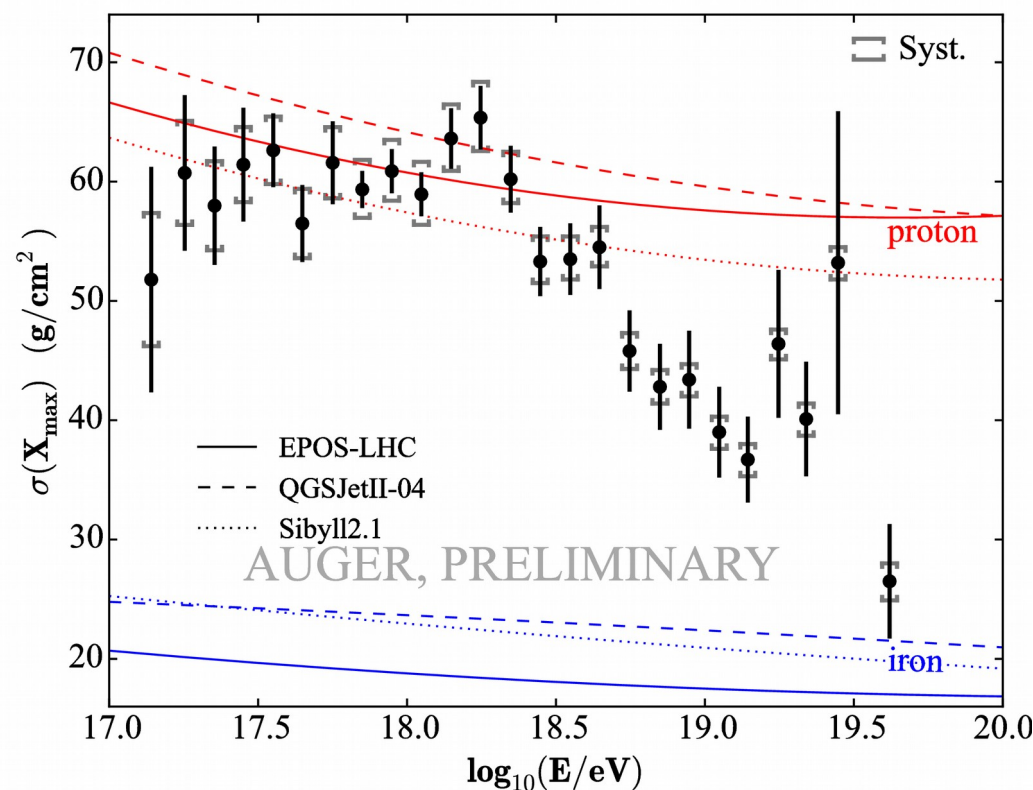
X_{\max} and S_{1000}

(Hybrid events)

Depth of maximum of air-shower profiles at the Pierre Auger Observatory. I. Measurements at energies above $10^{17.8}$ eV

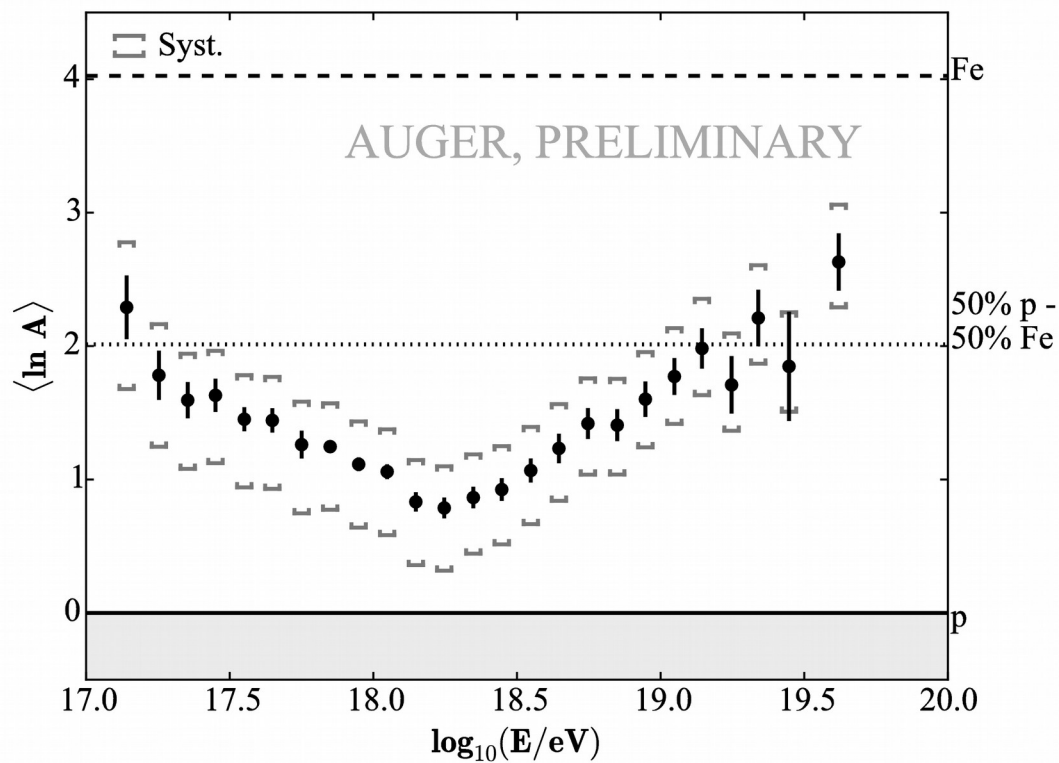


X_{\max} moments combining HEAT and standard FD measurements

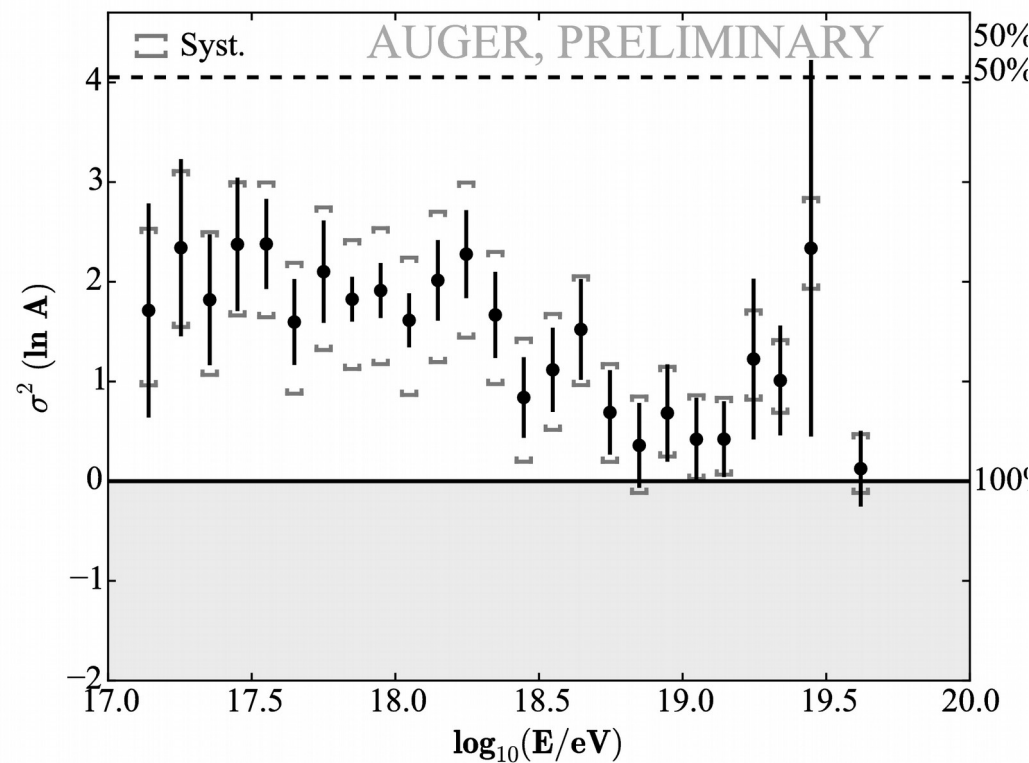
Average of X_{\max} Std. Deviation of X_{\max} 

Standard FD \rightarrow PHYSICAL REVIEW D **90**, 122005 (2014)

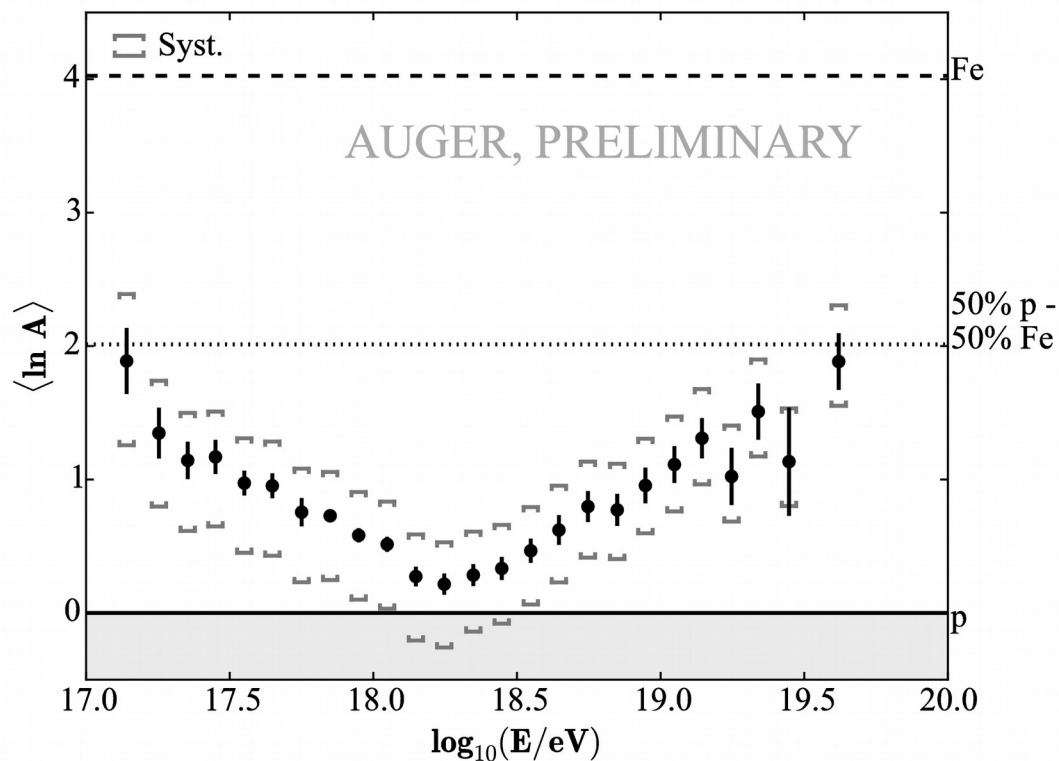
EPOS-LHC (Mean of ln A)



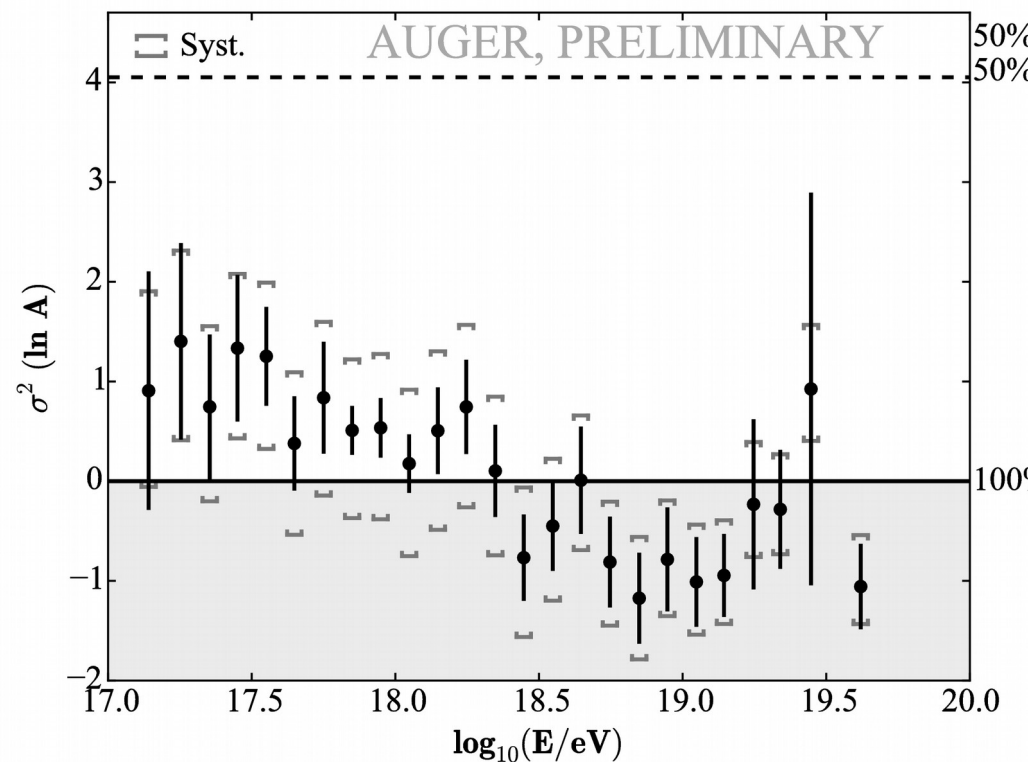
EPOS-LHC (Variance of ln A)

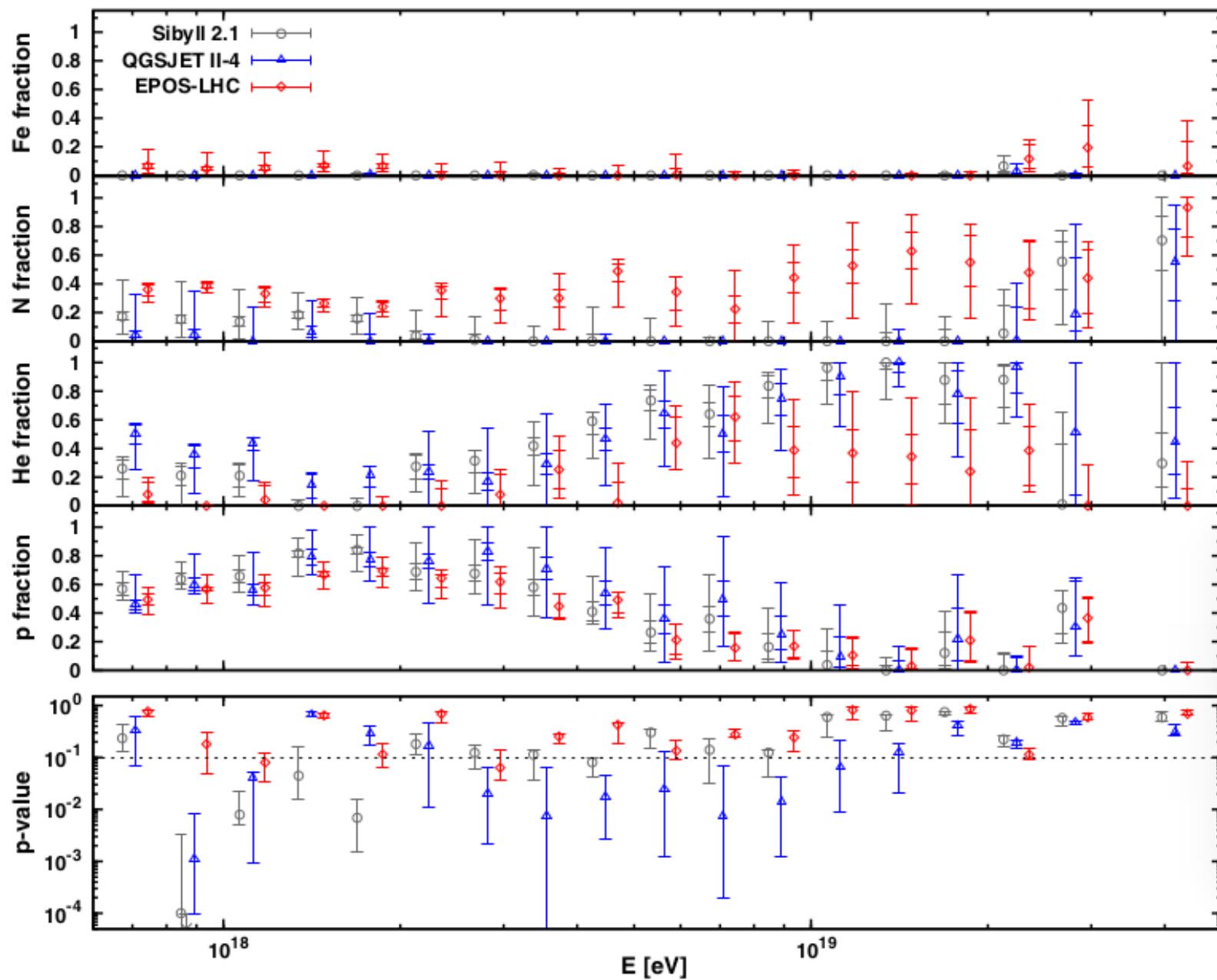


QGSJetII-04 (Mean of ln A)



QGSJetII-04 (Variance of ln A)







Muons in air showers at the Pierre Auger Observatory: Mean number in highly inclined events

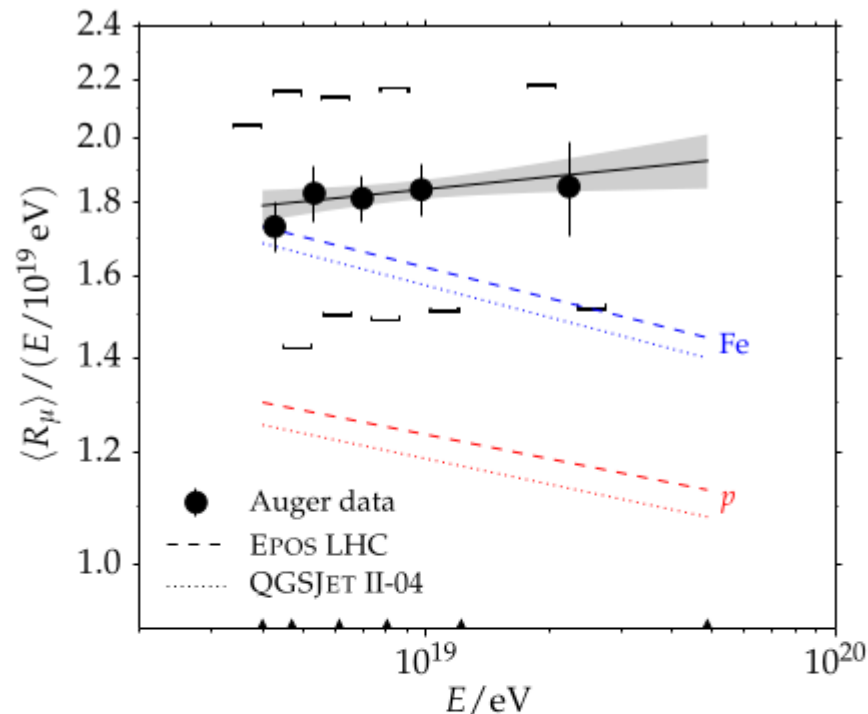


FIG. 4 (color online). Average muon content $\langle R_\mu \rangle$ per shower energy E as a function of the shower energy E in double logarithmic scale. Our data is shown bin by bin (circles) together with the fit discussed in the previous section (line). Square brackets indicate the systematic uncertainty of the measurement; the diagonal offsets represent the correlated effect of systematic shifts in the energy scale. The grey band indicates the statistical uncertainty of the fitted line. Shown for comparison are theoretical curves for proton and iron showers simulated at $\theta = 67^\circ$ (dotted and dashed lines). Black triangles at the bottom show the energy bin edges. The binning was adjusted by an algorithm to obtain equal numbers of events per bin.

Muons in air showers at the Pierre Auger Observatory: Measurement of atmospheric production depth

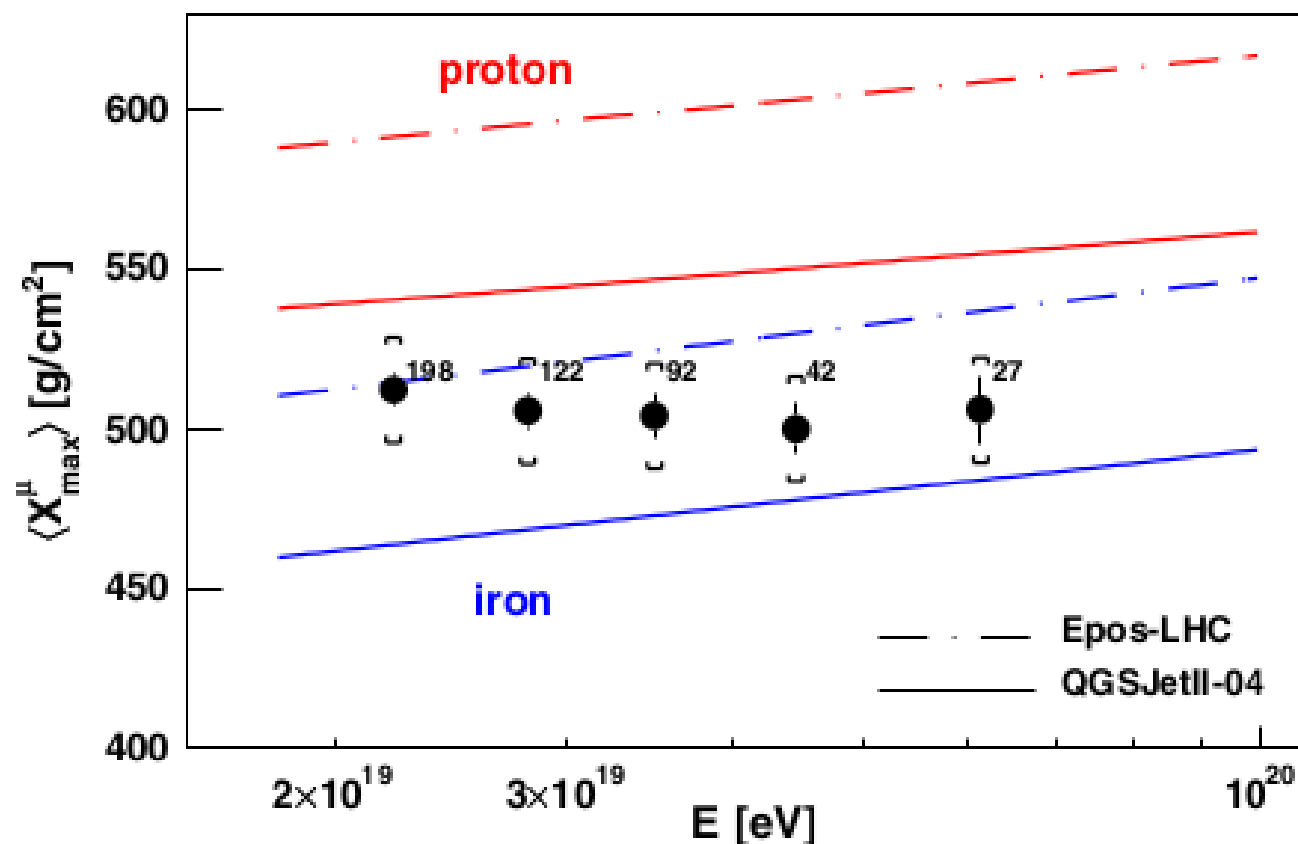
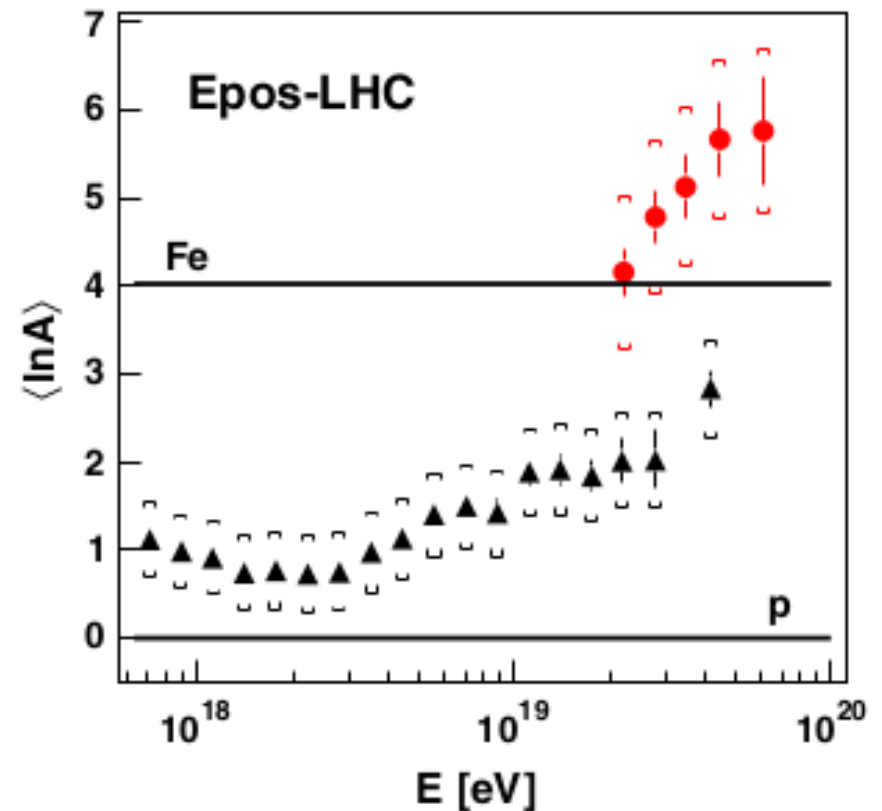
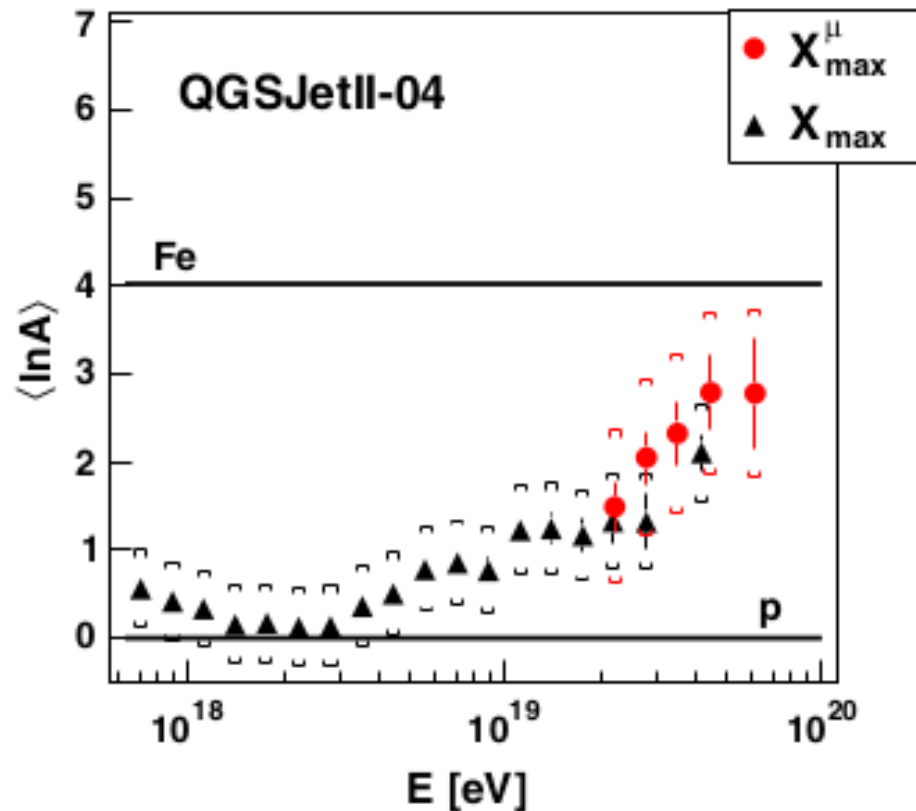


FIG. 8 (color online). $\langle X_{\text{max}}^{\mu} \rangle$ as a function of energy. The predictions of different hadronic models for protons and iron are shown. Numbers indicate the number of events in each energy bin, and brackets represent the systematic uncertainty.

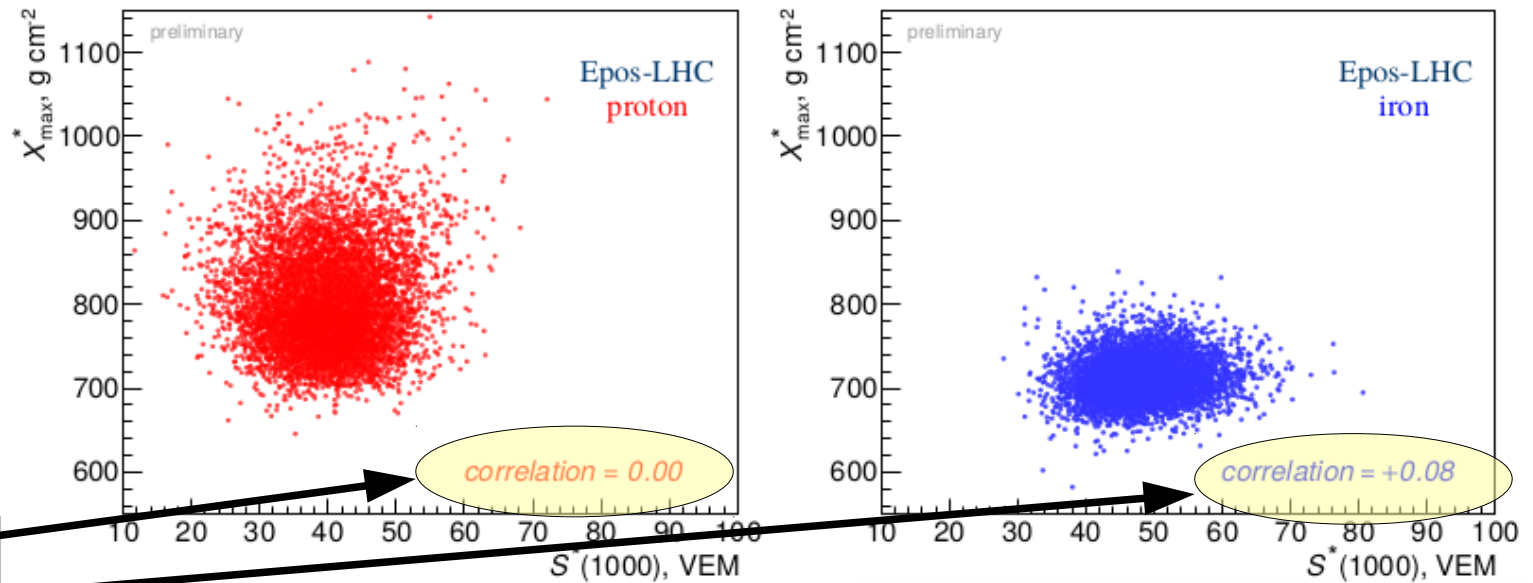
$\langle \ln A \rangle$ from X_{\max}^{μ} and X_{\max}



Inconsistency in the $\ln A$ estimates points out deficiencies of the hadronic interaction models.
Hadronic models have not been tested experimentally at these high energies

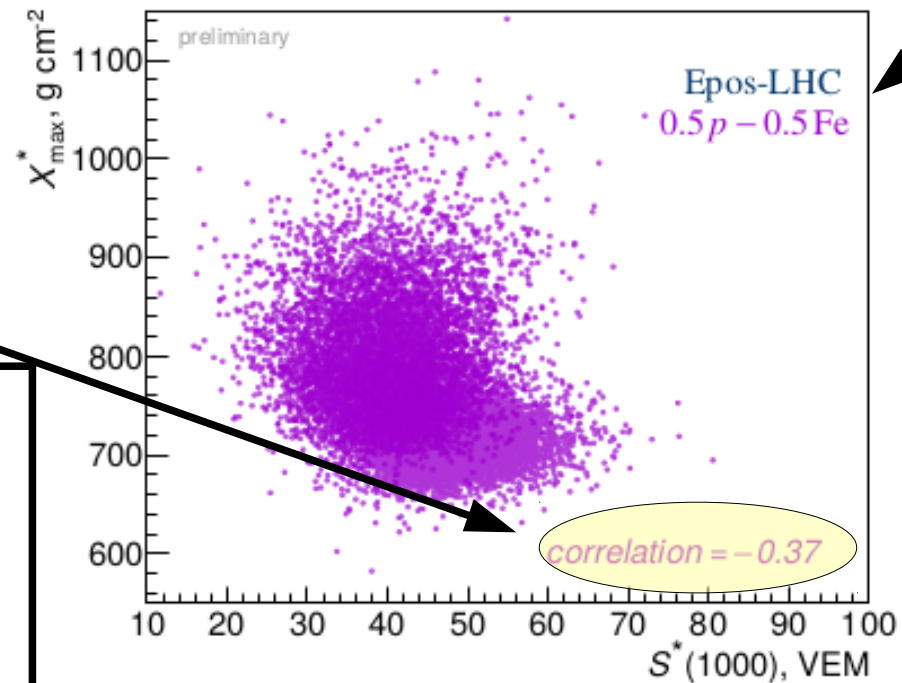
Correlation factor between:

X_{\max}^* and S_{1000}^*



For pure compositions
Correlation factor ≈ 0

For mixed compositions
Correlation factor $\neq 0$



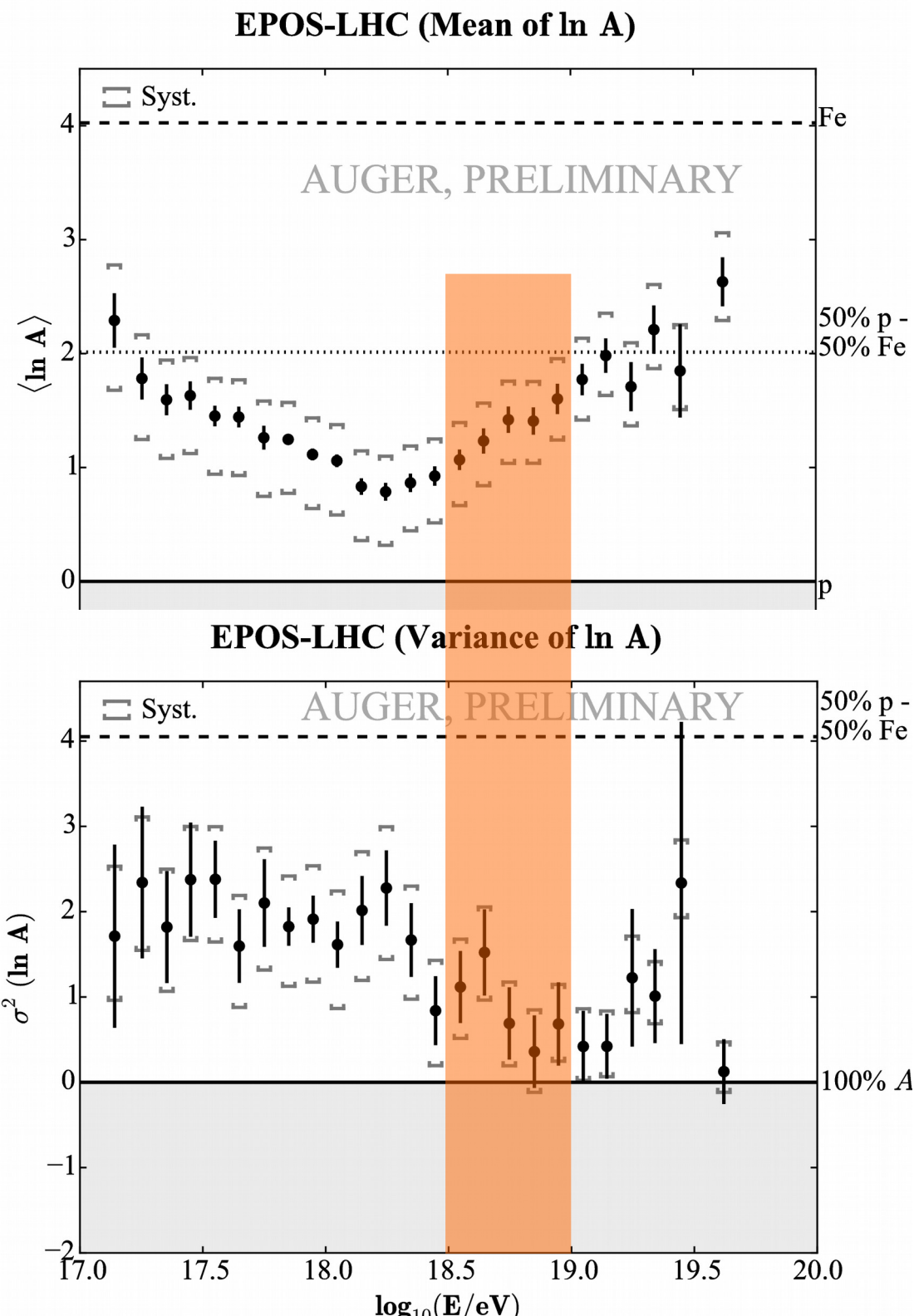
FD: depth of shower maximum, X_{\max} , scaled to 10 EeV
SD: signal at 1000 m from the core, $S_{(1000)}$, scaled to 10 EeV and 38° .

The scaled observables are used, they are marked with an asterisk

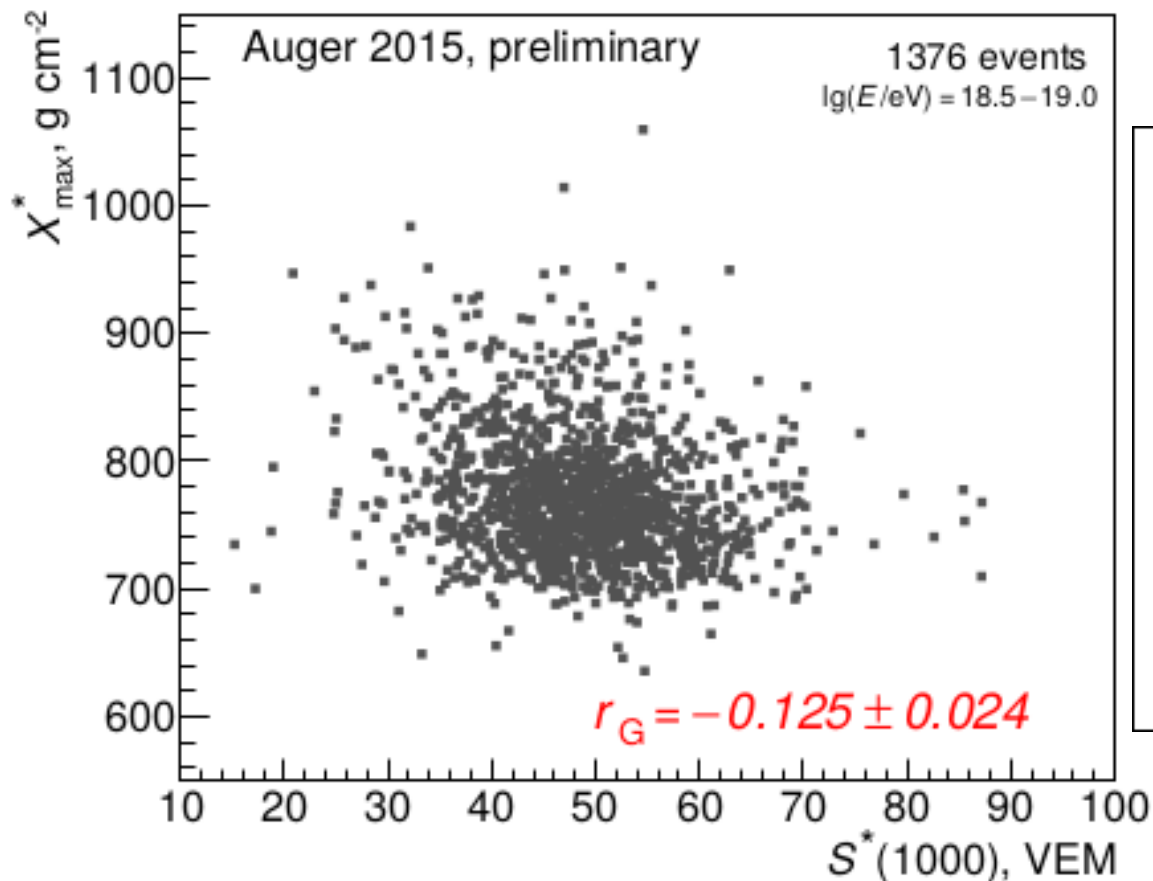
Data

Hybrid (FD and SD)

- 8 years 12/2004 – 12/2012
- $\lg(E/\text{eV}) = 18.5 - 19.0$
- zenith angles $0^\circ - 65^\circ$
- 1376 high-quality events



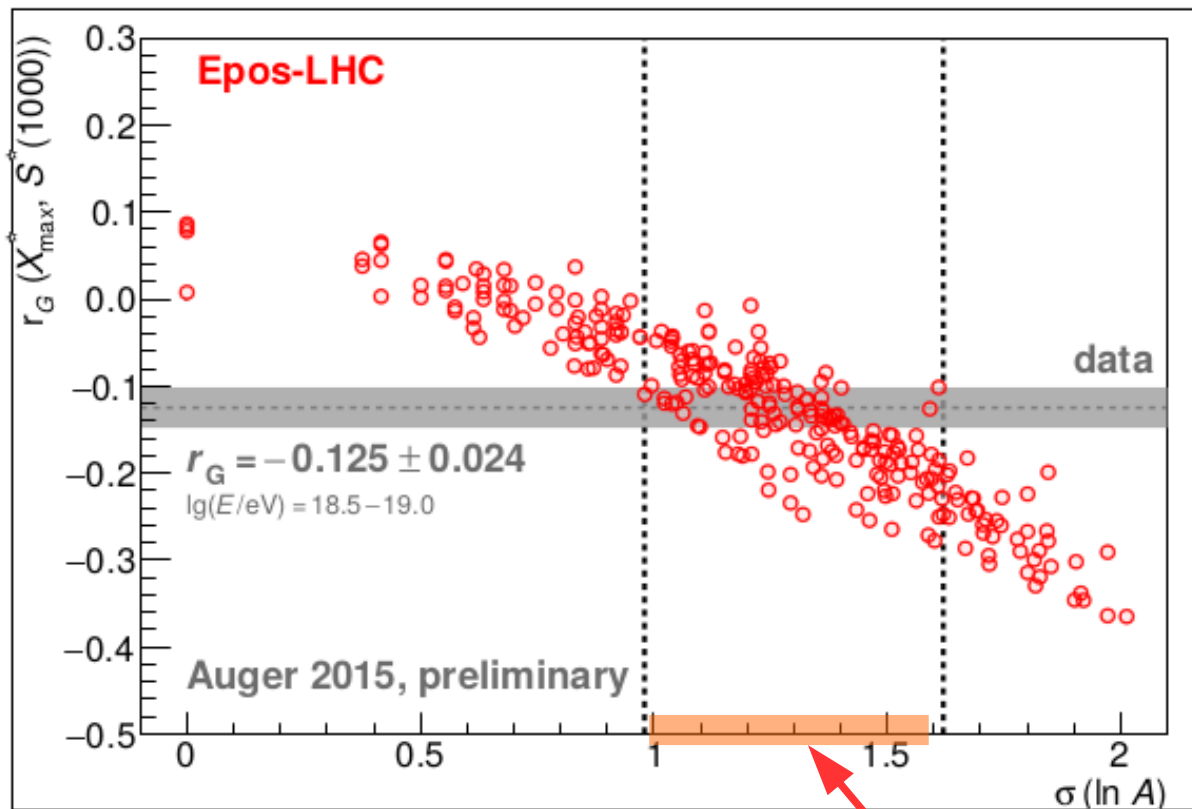
correlation is significantly negative



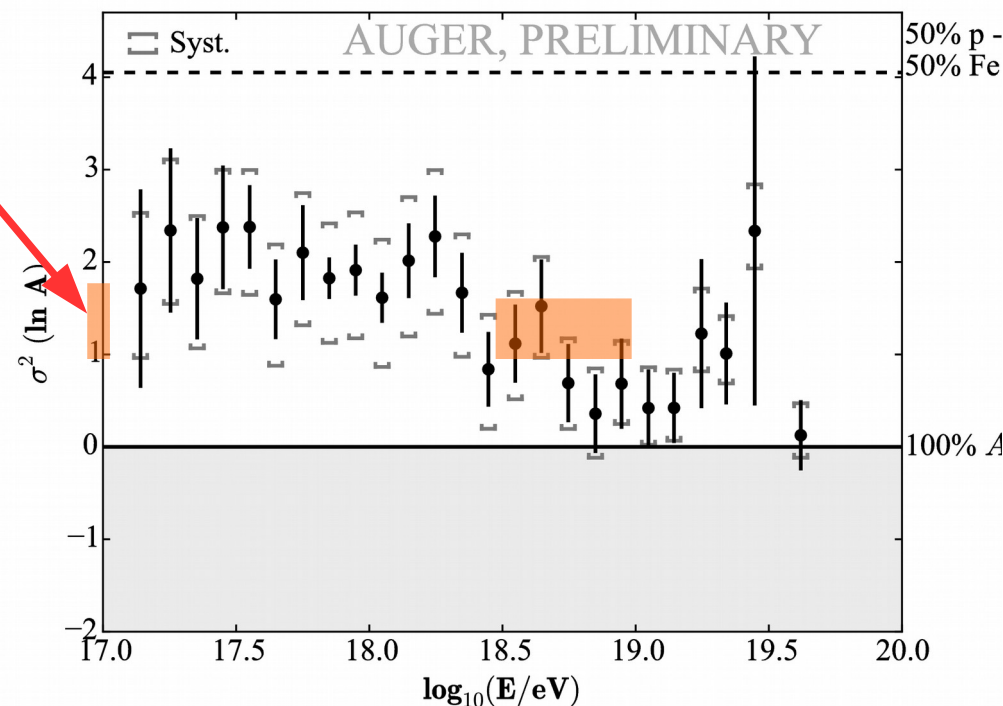
$r_G(X_{\max}^*, S^*(1000))$ for protons		
Epos-LHC	QGSJetII-04	Sibyll 2.1
0.00	+0.08	+0.07
difference to data		
$\approx 5\sigma$	$\approx 8\sigma$	$\approx 7.5\sigma$
difference is larger for other pure beams		

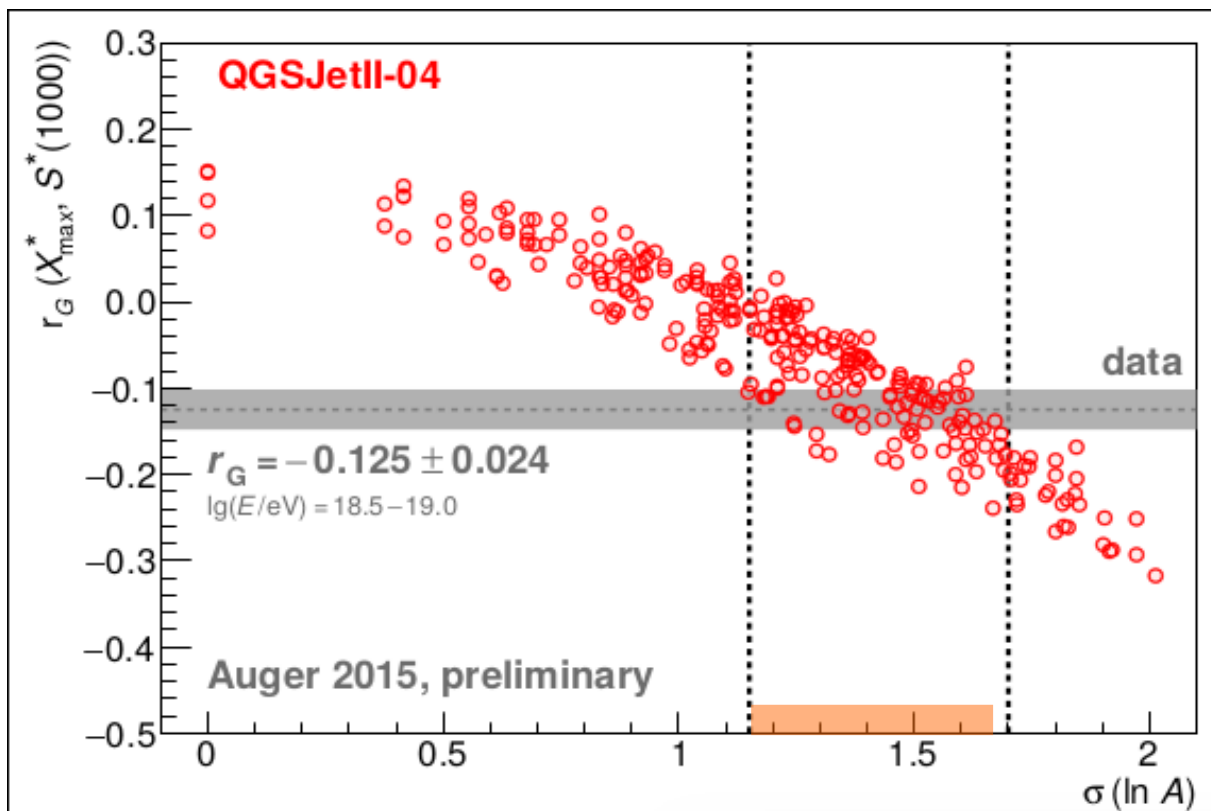
systematics plays only a minor role $\sigma_{\text{syst}}(r_G) \lesssim 0.01$
 due to invariance of r_G to additive and multiplicative scale transformations

**Data not consistent with
pure composition**

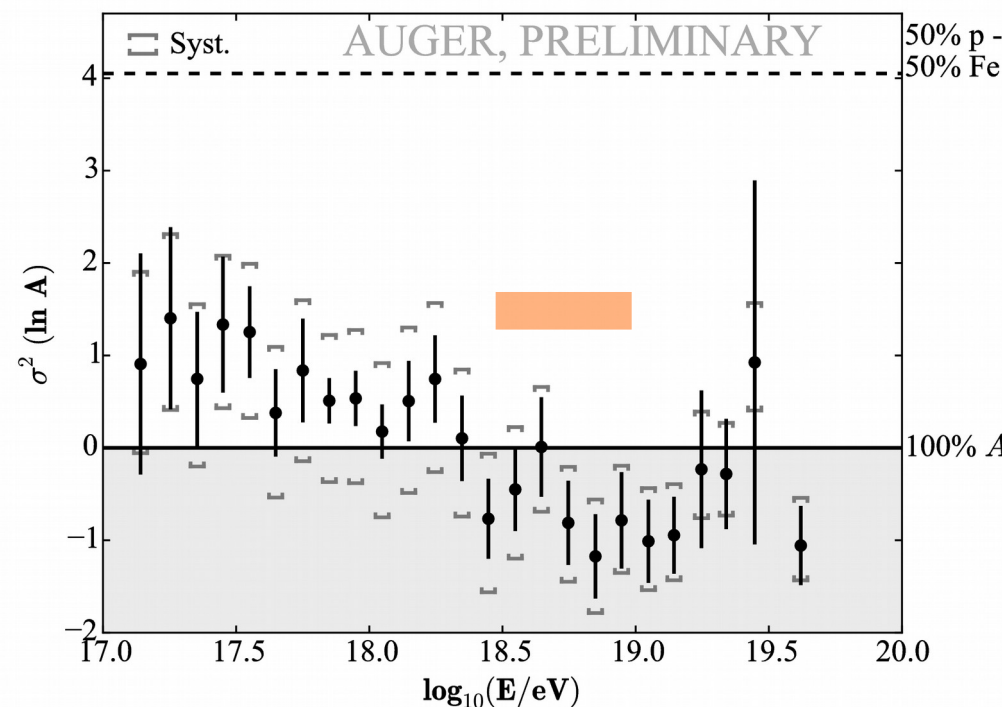


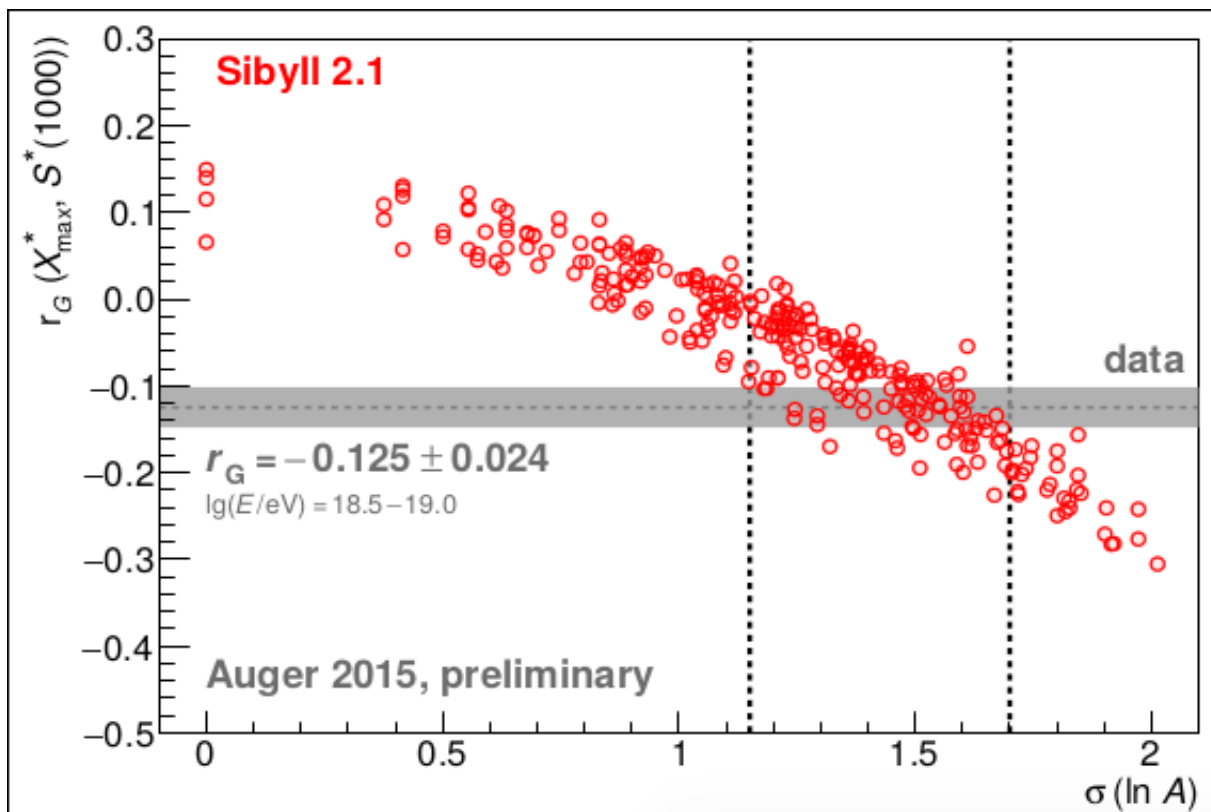
EPOS-LHC (Variance of $\ln A$)





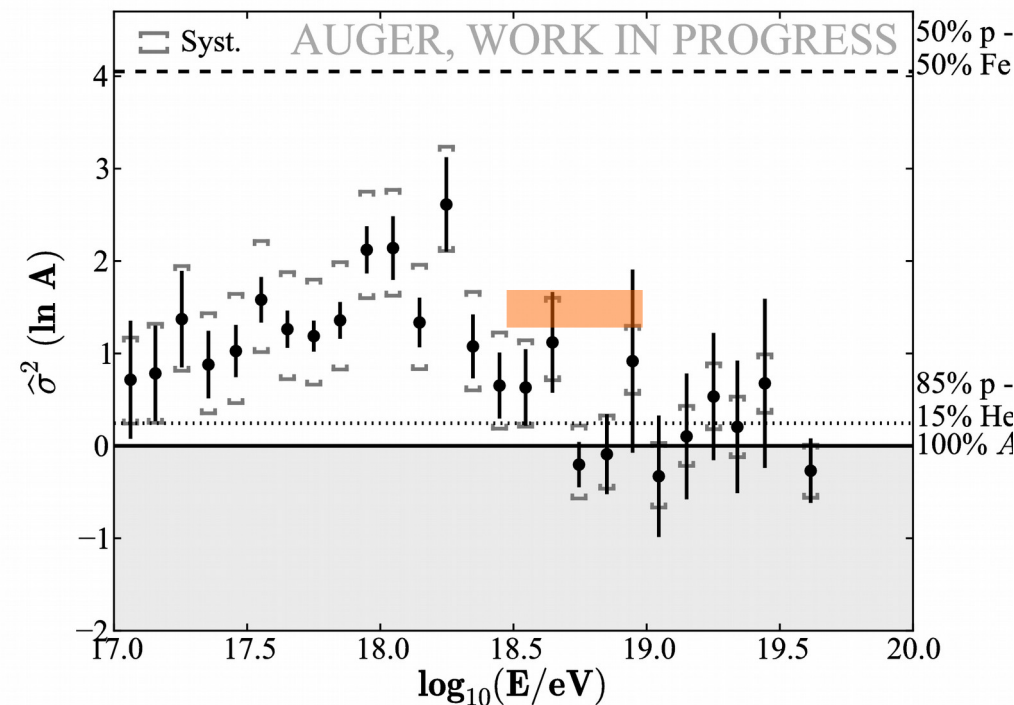
QGSJetII-04 (Variance of $\ln A$)



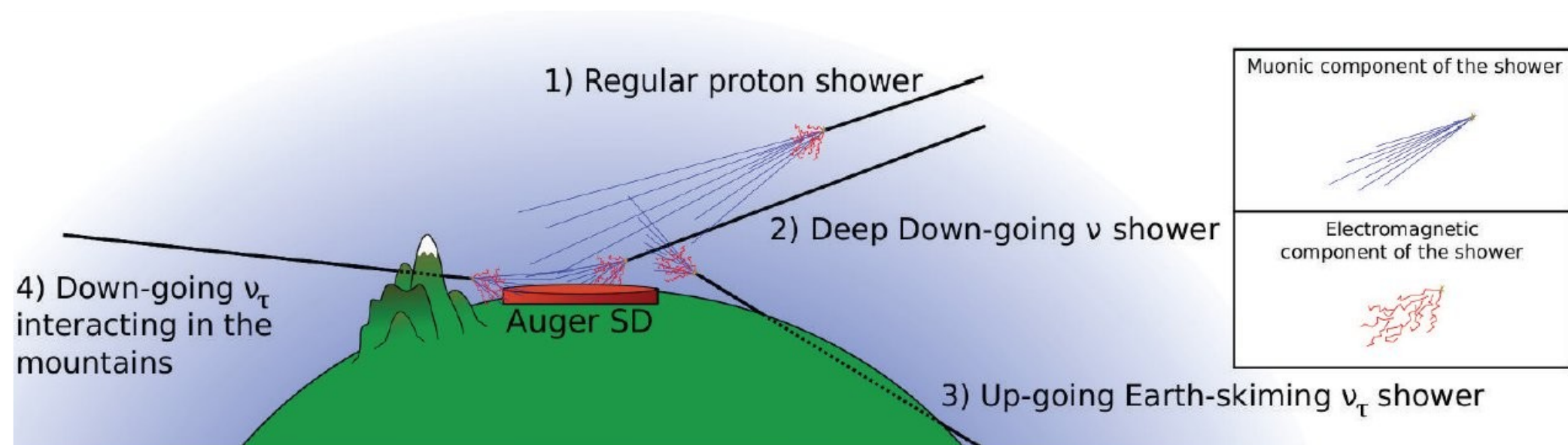


Sibyll2.1 (Std. Deviation of $\ln A$)

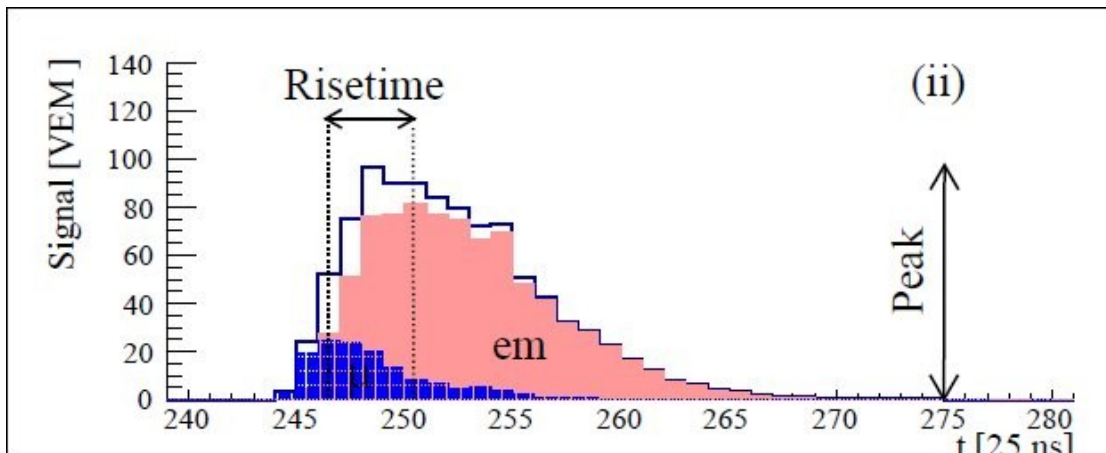
Interpretation of mass dispersion from S_{1000}, X_{\max} correlation is consistent with all models.



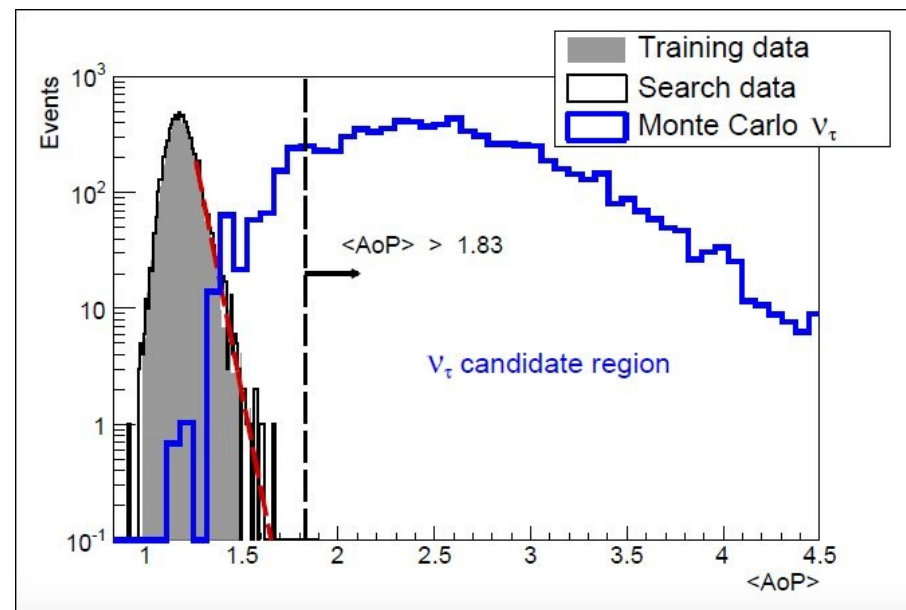
Sensitivity to neutrinos in Auger



Pulse shape and Risetime definition



Area over Peak



Flux upper limits for Neutrinos and Photons

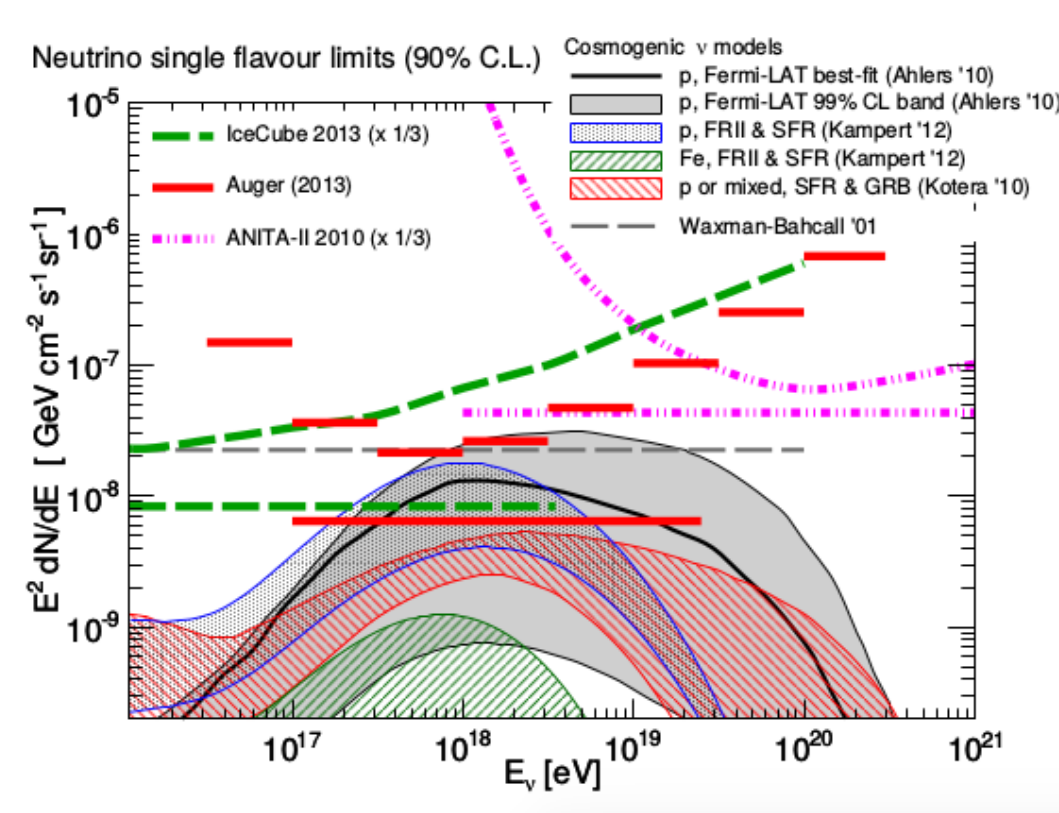


Figure 6: Upper limits to the diffuse flux of UHE neutrinos at 90% C.L. in integrated (horizontal lines) and differential form. Limits described in this work (red lines) are compared with cosmogenic neutrino models [16, 17, 18], the Waxman-Bahcall bound [19], and limits from IceCube [20] and ANITA [21]. All neutrino limits and fluxes are converted to single-flavour.

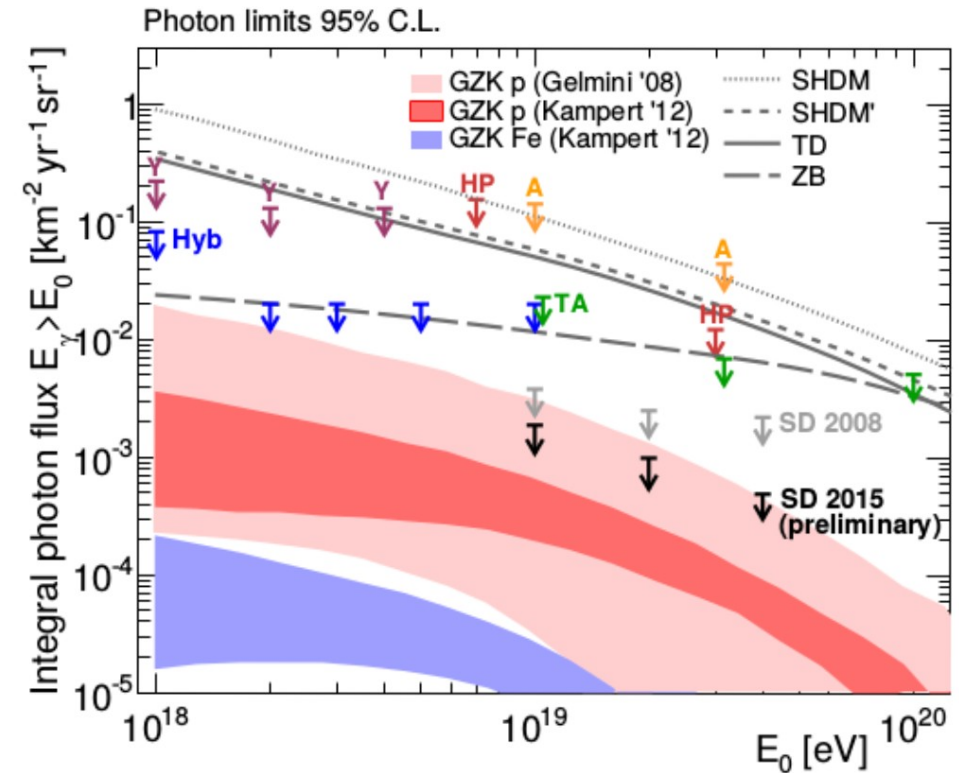
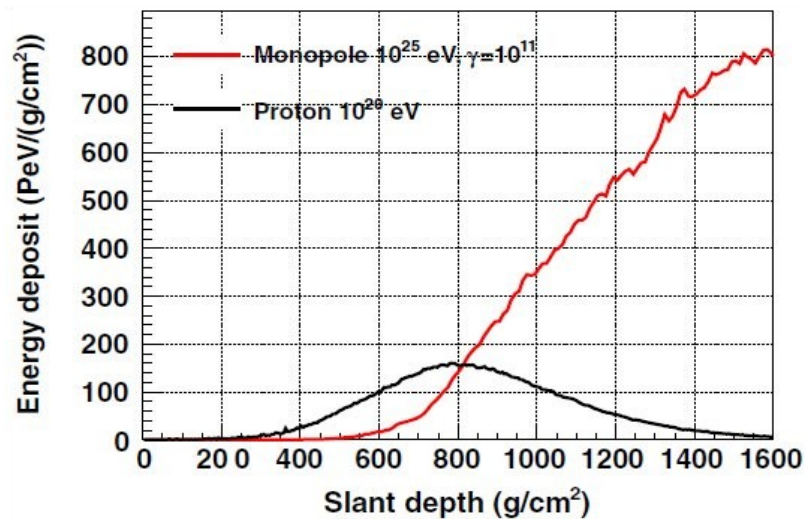


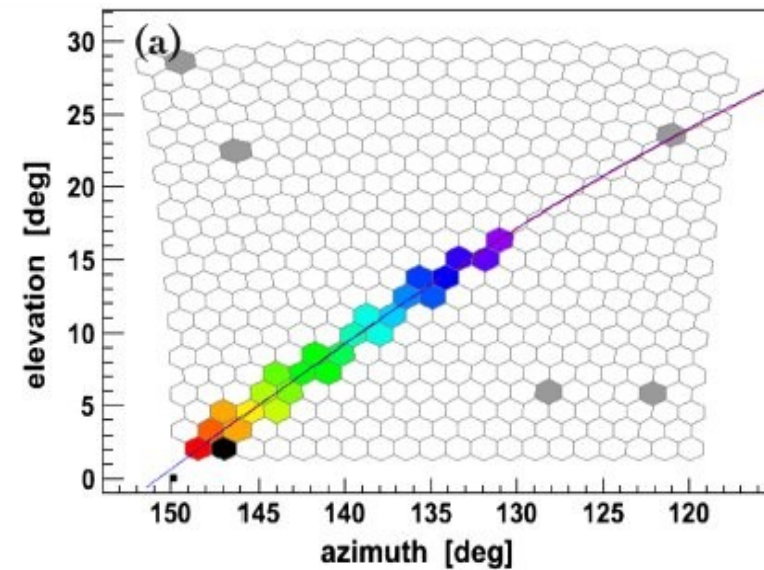
Figure 7: Upper limits at 95% C.L. to the diffuse flux of UHE photons derived in this work (black) shown together with previous results from the Pierre Auger Observatory with hybrid (Hyb) and SD data [22], Telescope Array (TA) [23], Yakutsk (Y) [24], Haverah Park (HP) [25], AGASA (A) [26] and predictions from several top-down [27, 28] and cosmogenic photon models [27, 17].

Magnetic Monopoles

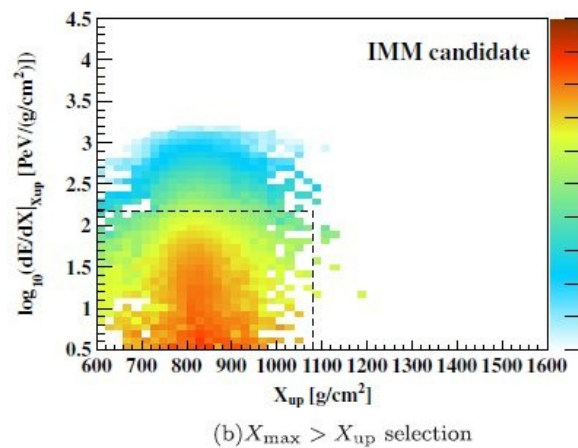
Simulations



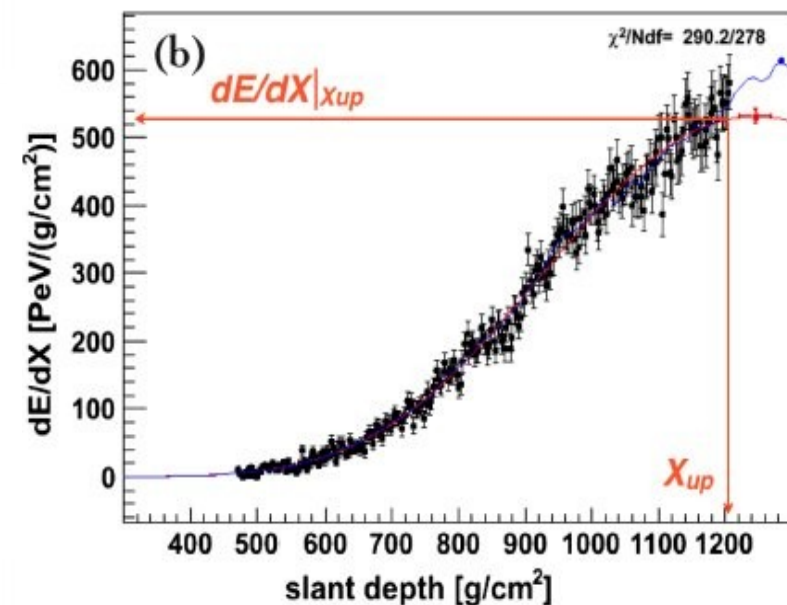
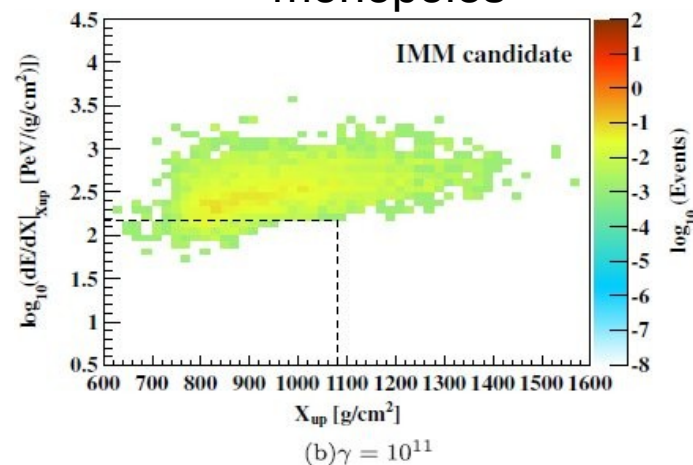
Reconstruction of monopole



protons

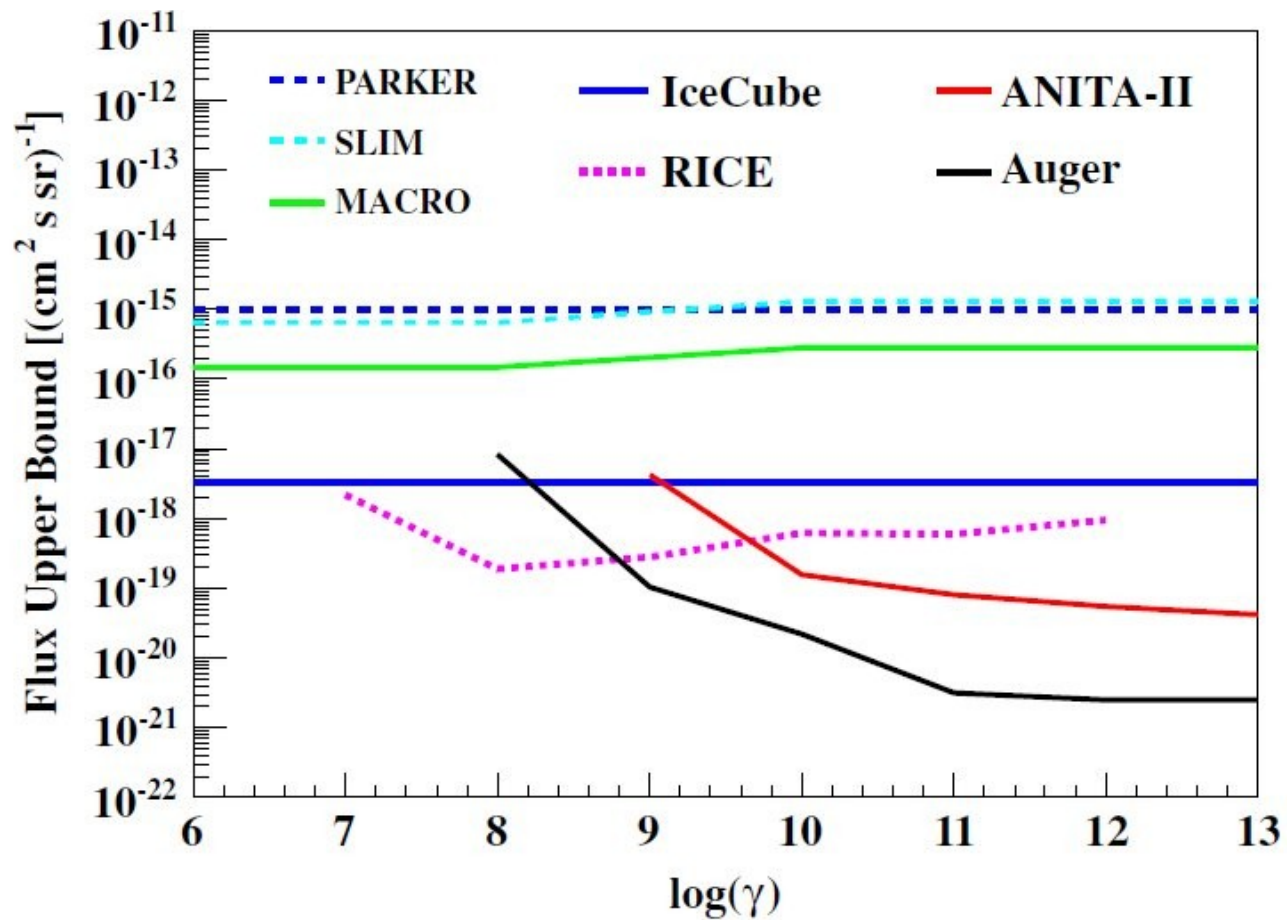


monopoles



Magnetic Monopoles

(flux upper limits)



PHYSICAL REVIEW D 94, 082002 (2016)

Summary

Energy Spectrum: Ankle and flux suppression consistent with GZK cutoff observed

Arrival directions: No significant correlation observed with nearby astrophysical objects. However, a significant *large scale anisotropy* (dipole type) has been observed at higher energies.

Mass Composition: - At around 10^{17} eV the composition is mixed and dominated by heavier elements.
- The composition gets lighter with energy and at $10^{18.3}$ it reaches it is dominated by lighter elements.
- Above $10^{18.3}$ the composition gets heavier with energy and the dispersion of masses is reduced.

Hadronic Models: High energy hadronic interaction models are not describing correctly the observed muonic component of air showers.

Photons/Neutrinos: No sources of high energy photons/neutrinos have been observed. Constraining upper limits for diffuse fluxes have been estimated.

Magnetic monopoles: No candidates have been observed. Auger large exposure allows to estimate the most constraining flux upper limits.

Future : The Auger collaboration has entered a new phase. New complementary detectors (scintillators on top of the water tanks and also buried underground) are being deployed. In addition a radio antennas array have been deployed. The aim to record **precise measurements of the electromagnetic and muonic components of the air showers**. This will help to understand the deficiencies observed in the hadronic models.

Correlation between X_{\max}^* and $S^*(1000)$

Ranking coefficient r_G [R. Gideon, R. Hollister, JASA 82 (1987) 656]

① rank events in X_{\max}^* and $S^*(1000)$

② replace measured values by ranks:

$$X_{\max}^*(1), \dots, X_{\max}^*(N) \Rightarrow 1, 2, \dots, N$$

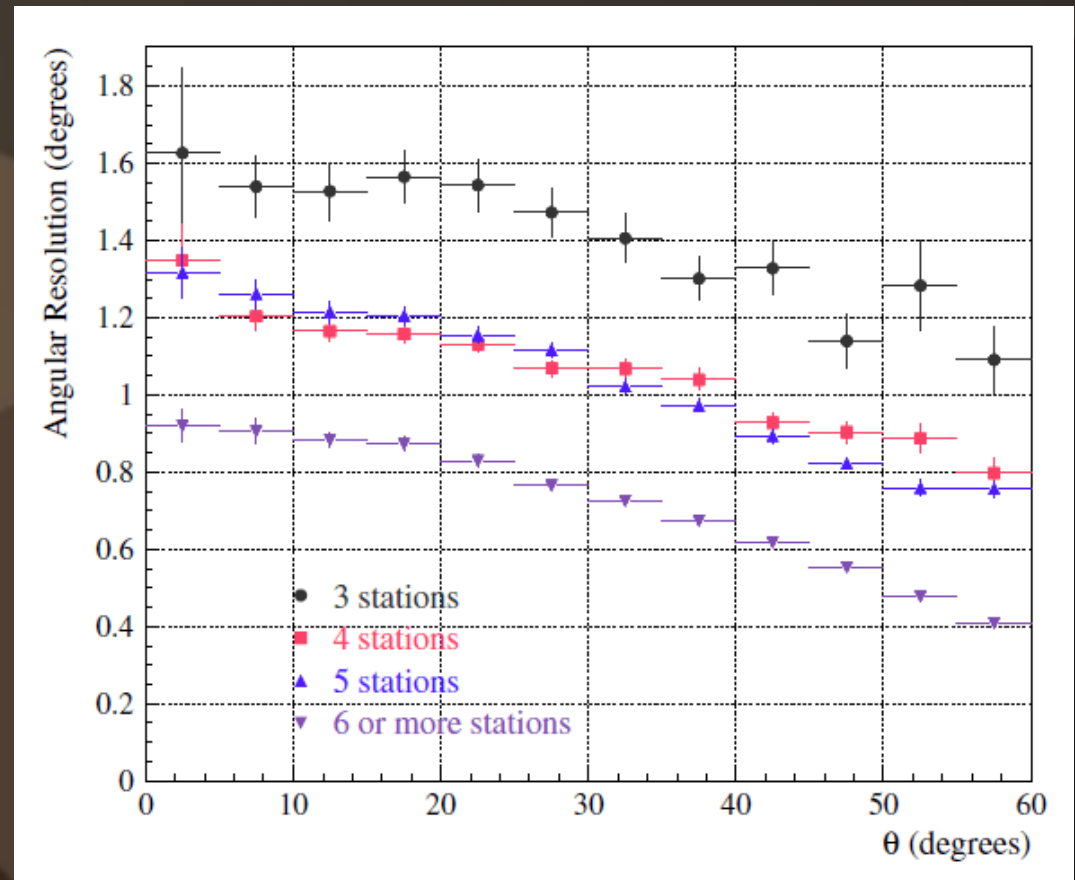
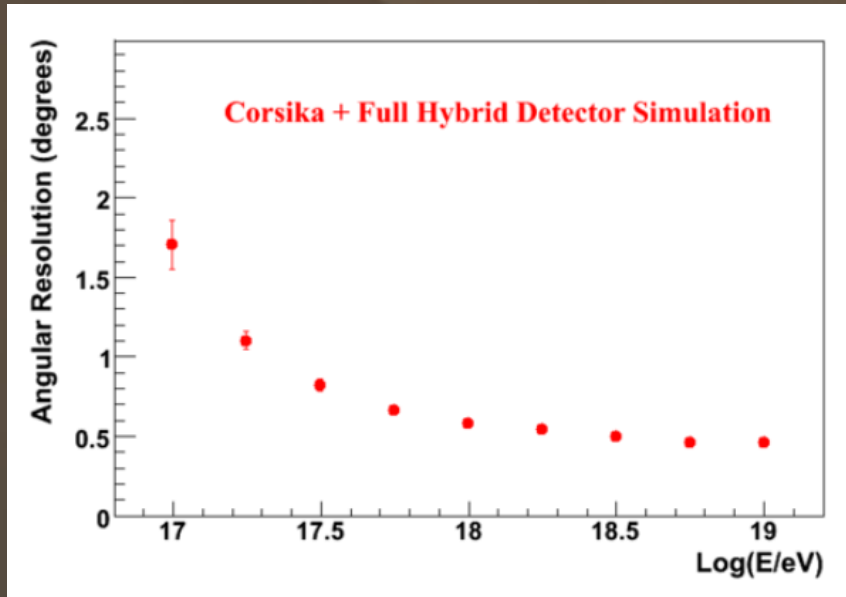
$$S^*(1000)(1), \dots, S^*(1000)(N) \Rightarrow 1, 2, \dots, N$$

③ count events with ranks deviating from the expectations for perfect (anti-)correlation; all events contribute 0 or 1 \Rightarrow robustness against outliers

r_G is invariant to any transformations leaving ranks unchanged
e.g. to systematics in X_{\max}^* and $S^*(1000)$

various coefficients applied (incl. Pearson, Spearman), conclusions unchanged

Angular Resolution



Hybrid Angular resolution
(68% CL)
0.5 degrees above 1EeV

Surface array Angular resolution (68% CL)
< 1.6° for 3 station events ($E > 3\text{EeV}$, $\theta < 60^\circ$)
< 1.2° for 4 station events
< 0.9° for 6 or more station events

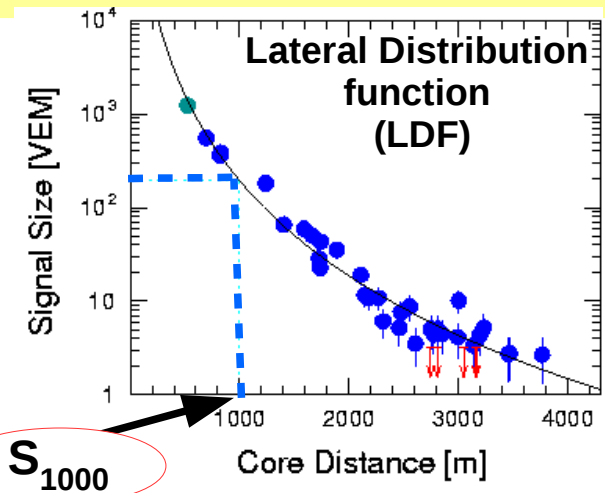
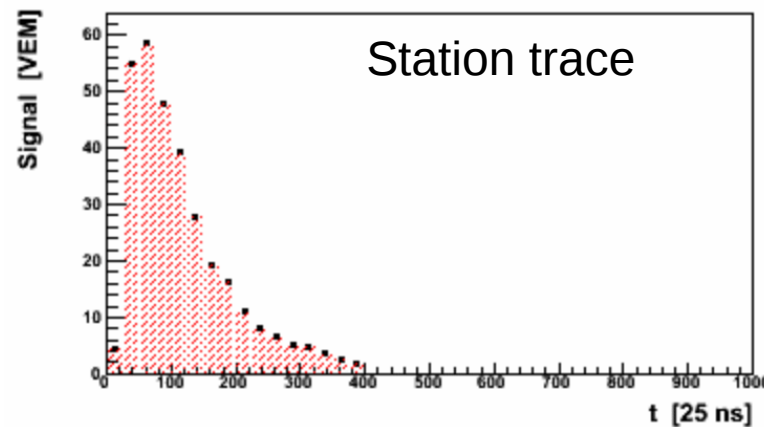
Event Reconstruction

Arrival direction, energy and mass

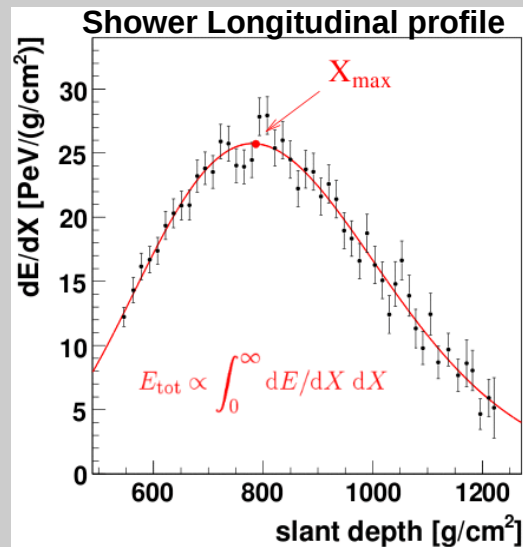
Geometry (arrival direction)

- from timing and position information of the triggered SD stations.
- For the subset of events that also triggered the FD (hybrid events): from pixel timing, pixel FOV direction and position and timing of only the brightest SD station.

With SD



With FD

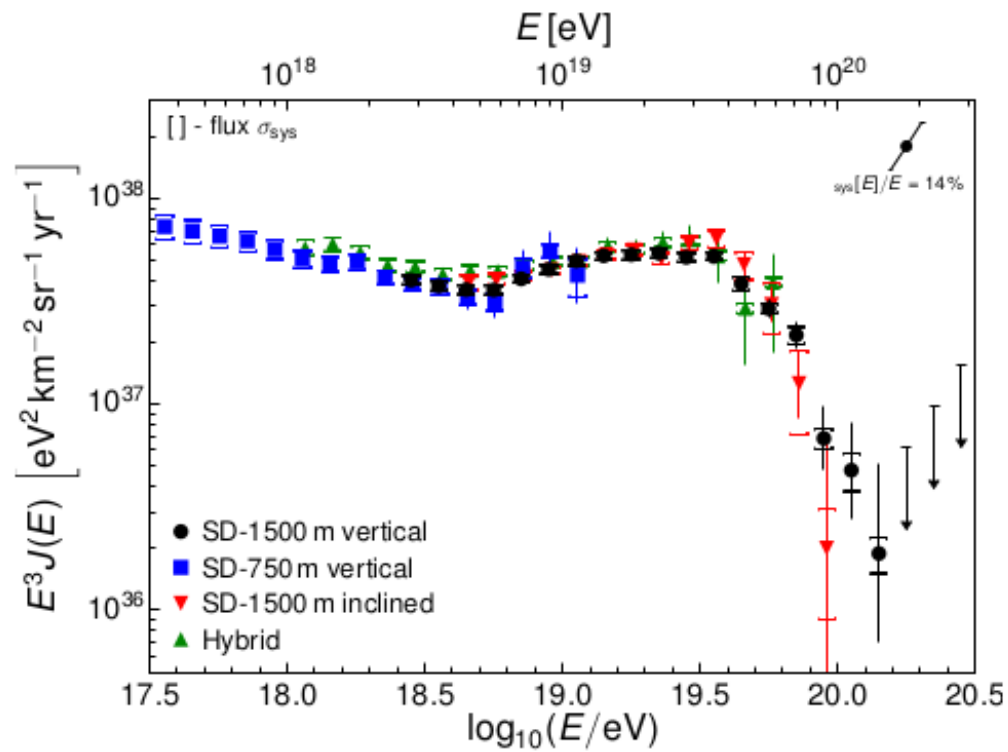


The X_{max} resolution is in average 20 g/cm²

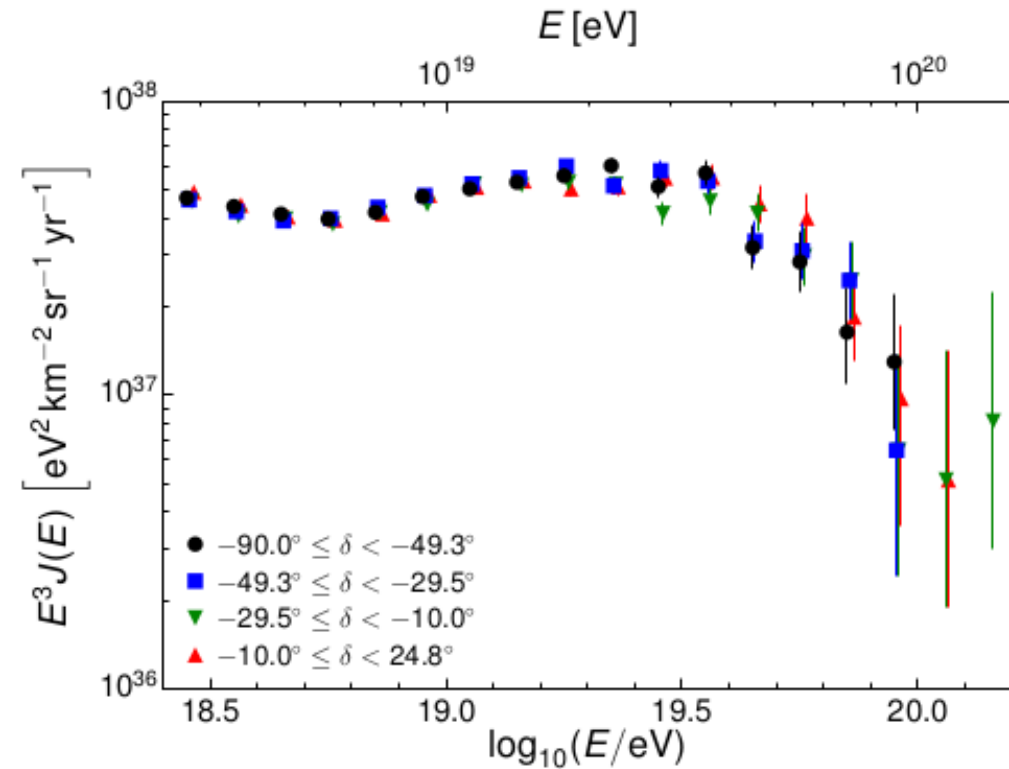
Calorimetric metric measurement of the energy

The Cosmic Ray Energy Spectrum

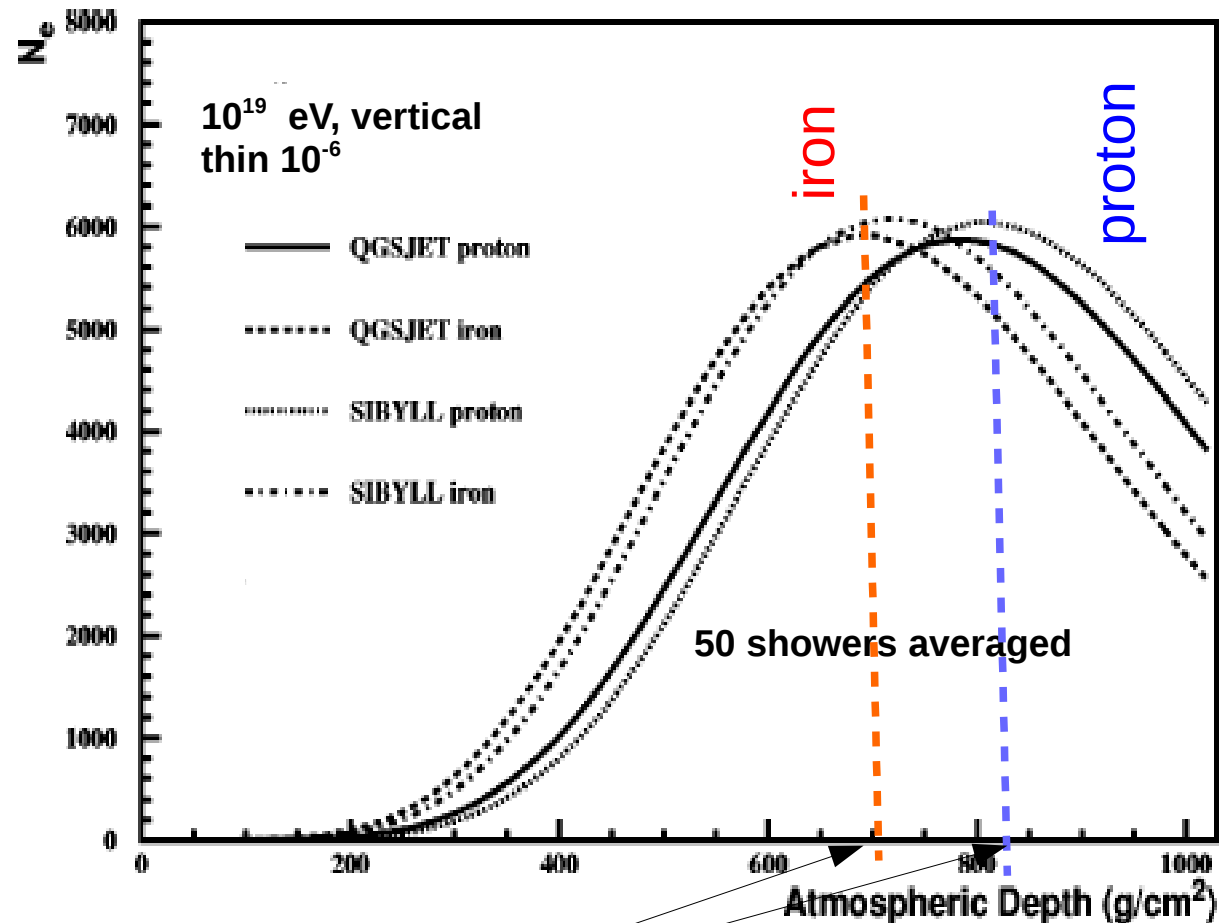
Four independent measurements



Declination dependence

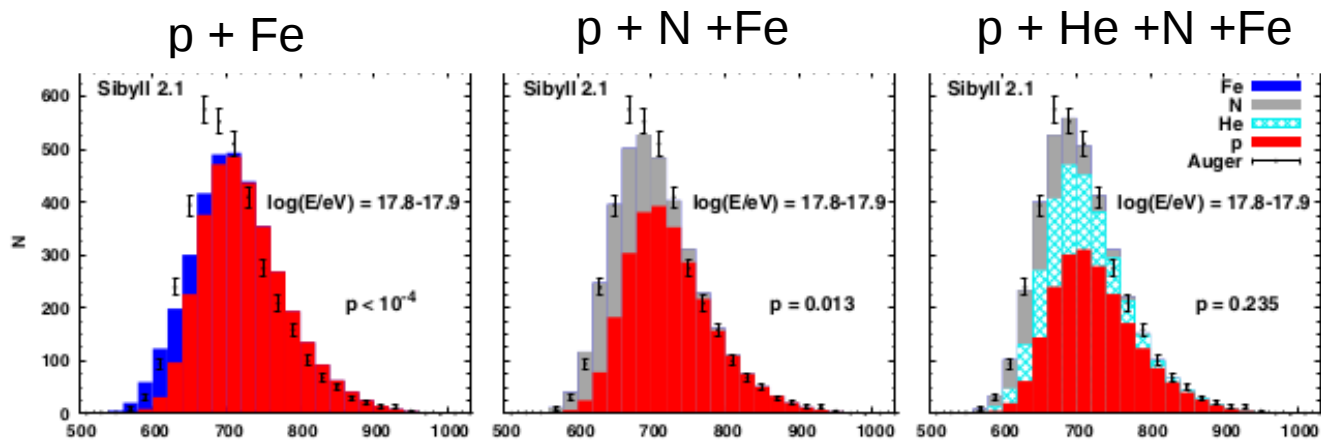


The expected shower profile (measured by the FD) for proton and Iron are different

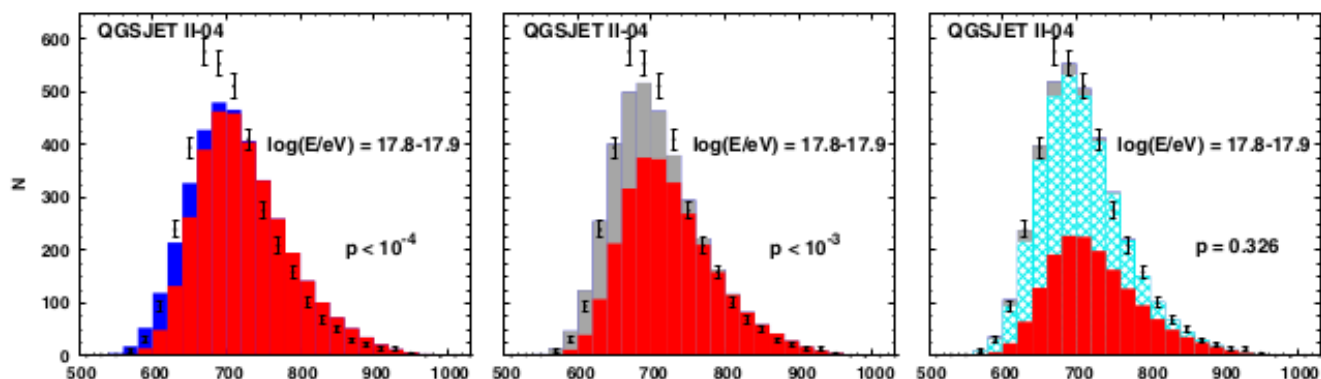


Note: X_{max} is used to characterize the shower profile.

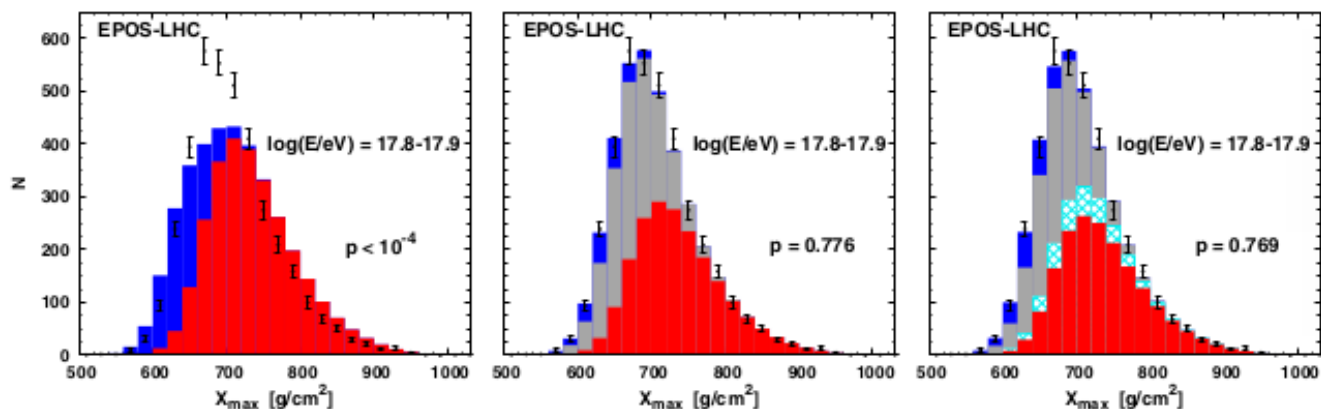
Sibyll 2.1



QGSJET II-04

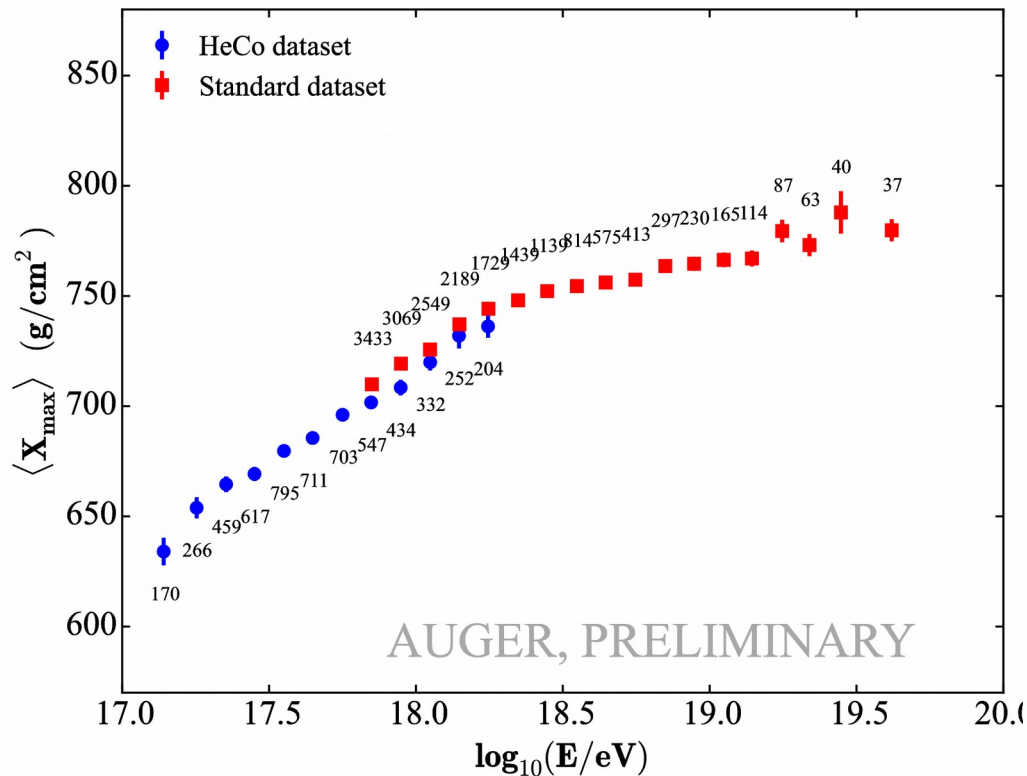


EPOS-LHC

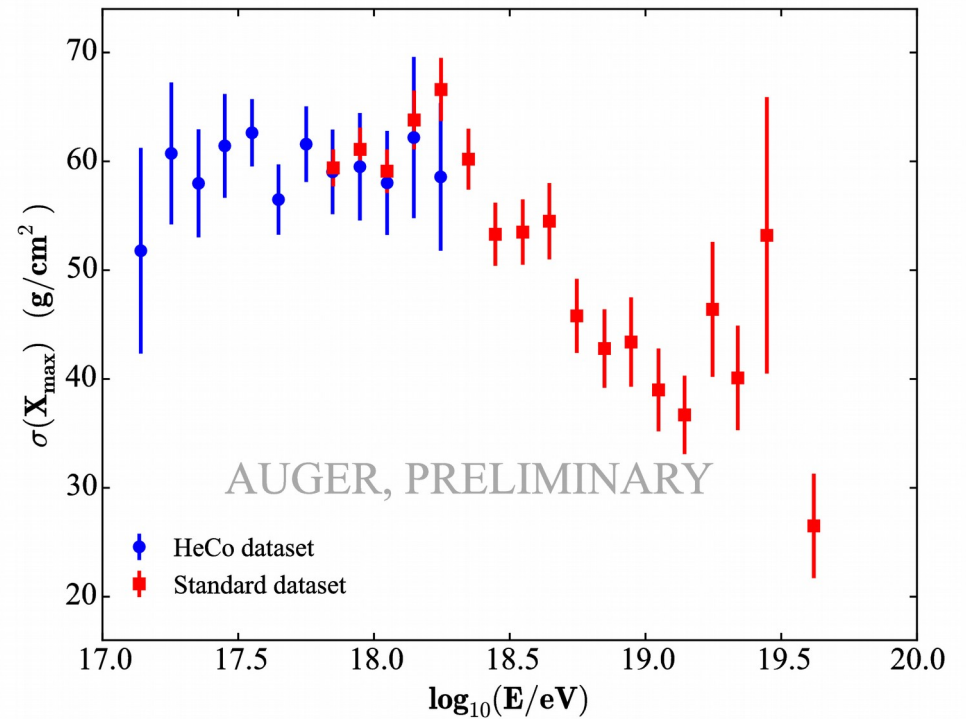


X_{\max} moments from HEAT and from standard FD measurements

Average of X_{\max}

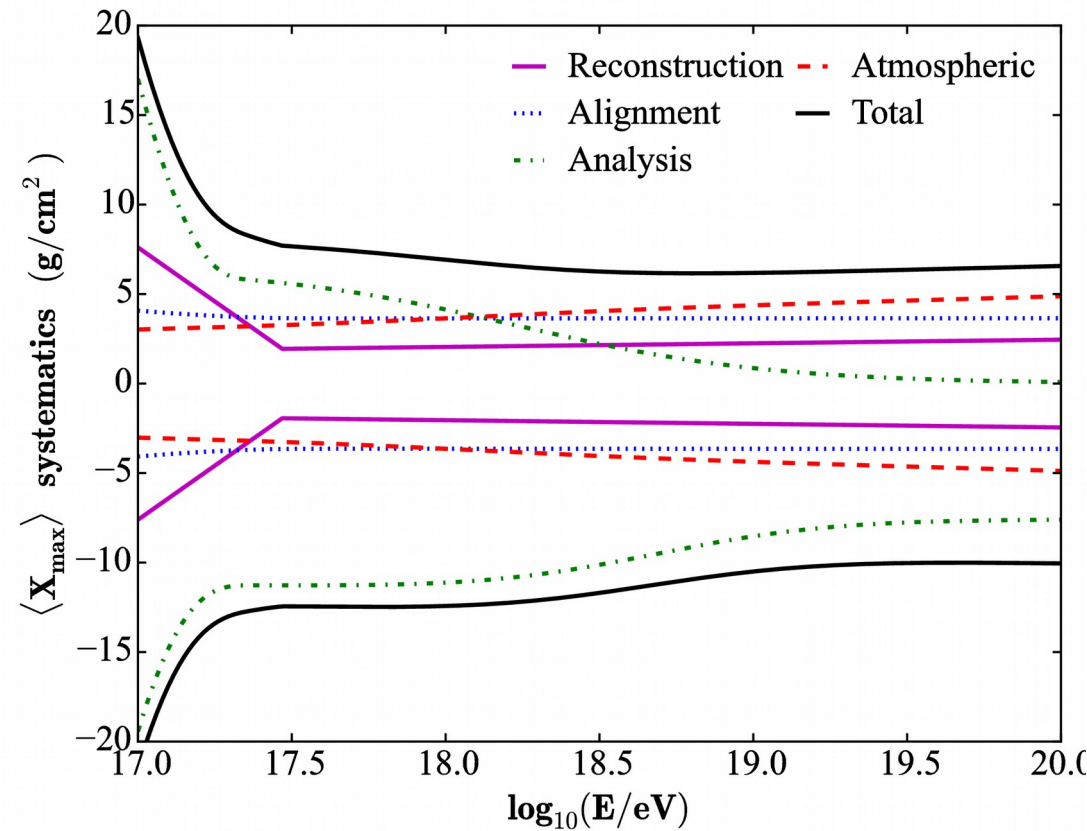
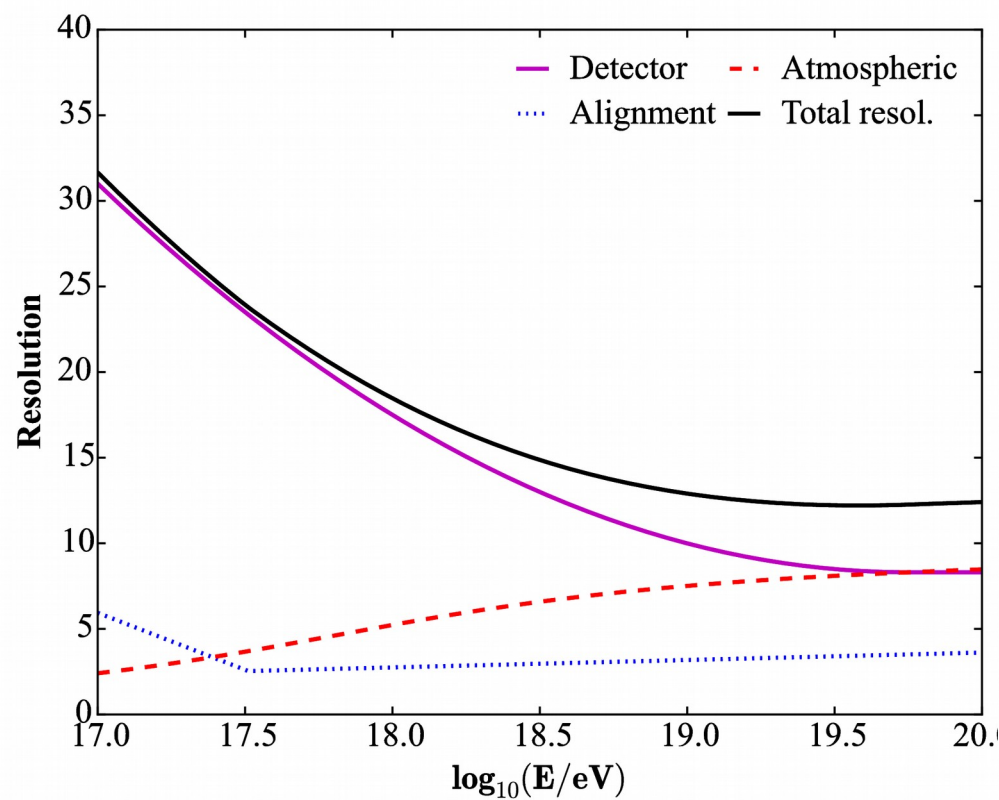


Std. deviation of X_{\max}



Standard FD \rightarrow PHYSICAL REVIEW D **90**, 122005 (2014)

Resolution and systematics of the reconstructed X_{\max} for HEAT

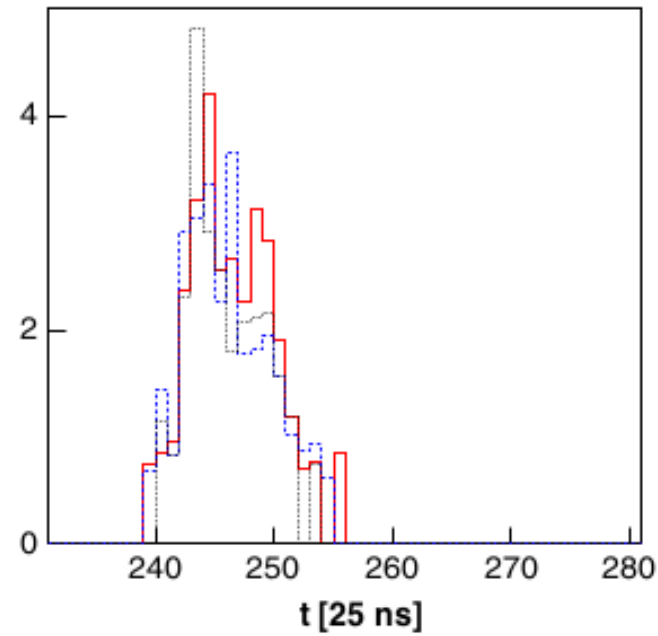


Note: The detector resolution is estimated using simulations.

X^μ_{max}

SD trace

VEM



MPD profile

dN_μ/dX [a.u.]

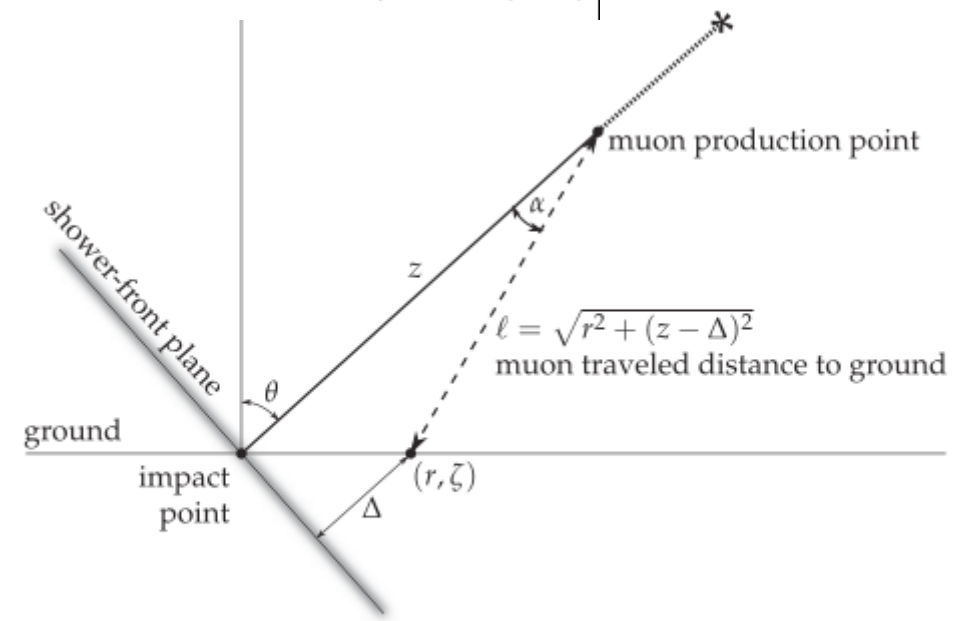
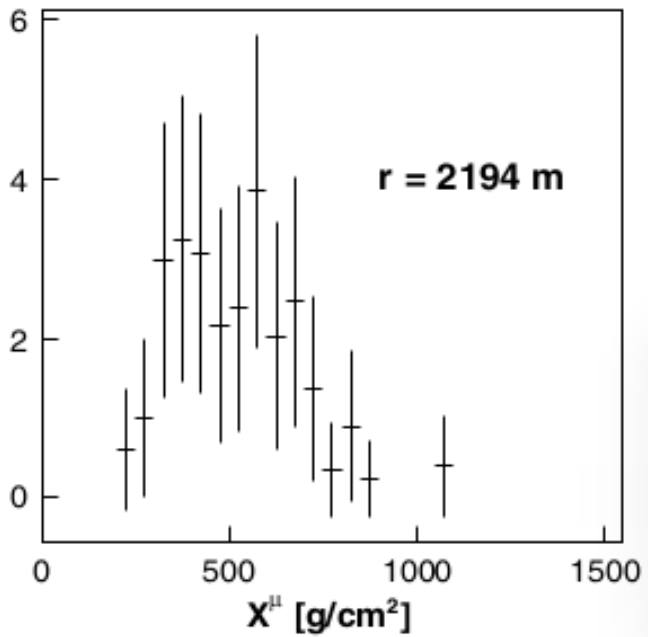


FIG. 1. Geometry used to obtain the muon traveled distance and the time delay.

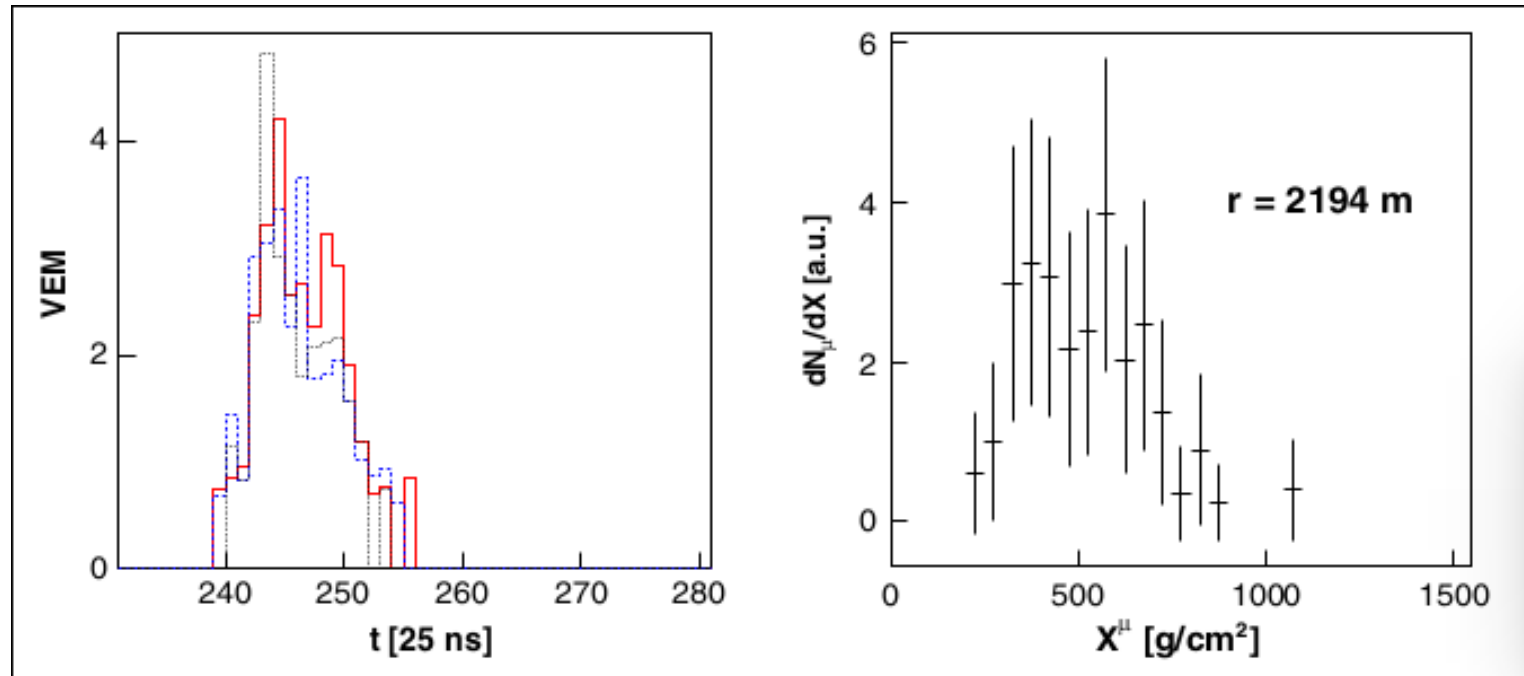
$$z \simeq \frac{1}{2} \left(\frac{r^2}{c(t - \langle t_e \rangle)} - c(t - \langle t_e \rangle) \right) + \Delta - \langle z_\pi \rangle, \quad (1)$$

where the geometric delay t_g has been approximated by $t_g \simeq t - \langle t_e \rangle$.

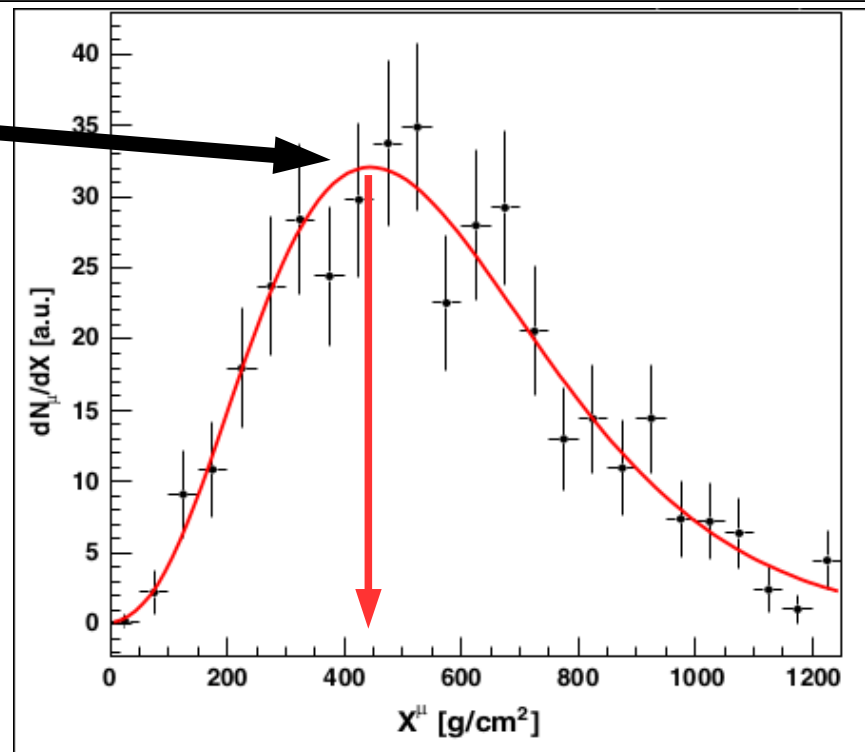
For each point at the ground, Eq. (1) gives a mapping between the production distance z and the arrival time t of muons. The production distance can be easily related to the production depth X^μ (total amount of traversed matter) using

$$X^\mu = \int_z^\infty \rho(z') dz', \quad (2)$$

Muon Production Depths (MPD) profiles



X^{μ}_{max}



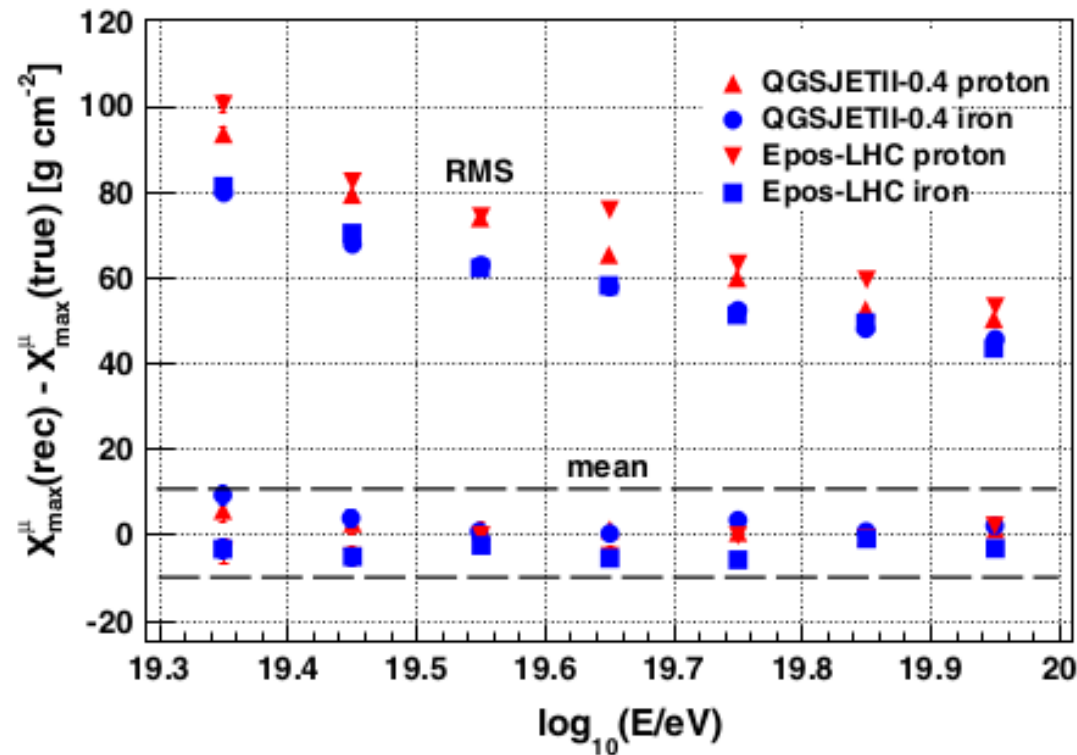


TABLE II. Evaluation of the main sources of systematic uncertainties in X_{max}^{μ} .

Source	Sys. uncertainty [g/cm ²]
Reconstruction, hadronic model and primary	10
Seasonal effect	12
Time variance model	5
Total	17

FIG. 7 (color online). Evolution with energy of the mean and rms of the distribution $X_{\text{max}}^{\mu}(\text{reconstructed}) - X_{\text{max}}^{\mu}(\text{true})$. The simulations were made using the QGSJETII-04 [30] and EPOS-LHC hadronic models for protons and iron nuclei for $55^{\circ} \leq \theta \leq 65^{\circ}$. Dashed lines indicate the final systematic uncertainty bounds due to the reconstruction effects, different hadronic models, and primary particles.

Expected X_{\max}^{μ} distribution for **proton** and **iron**

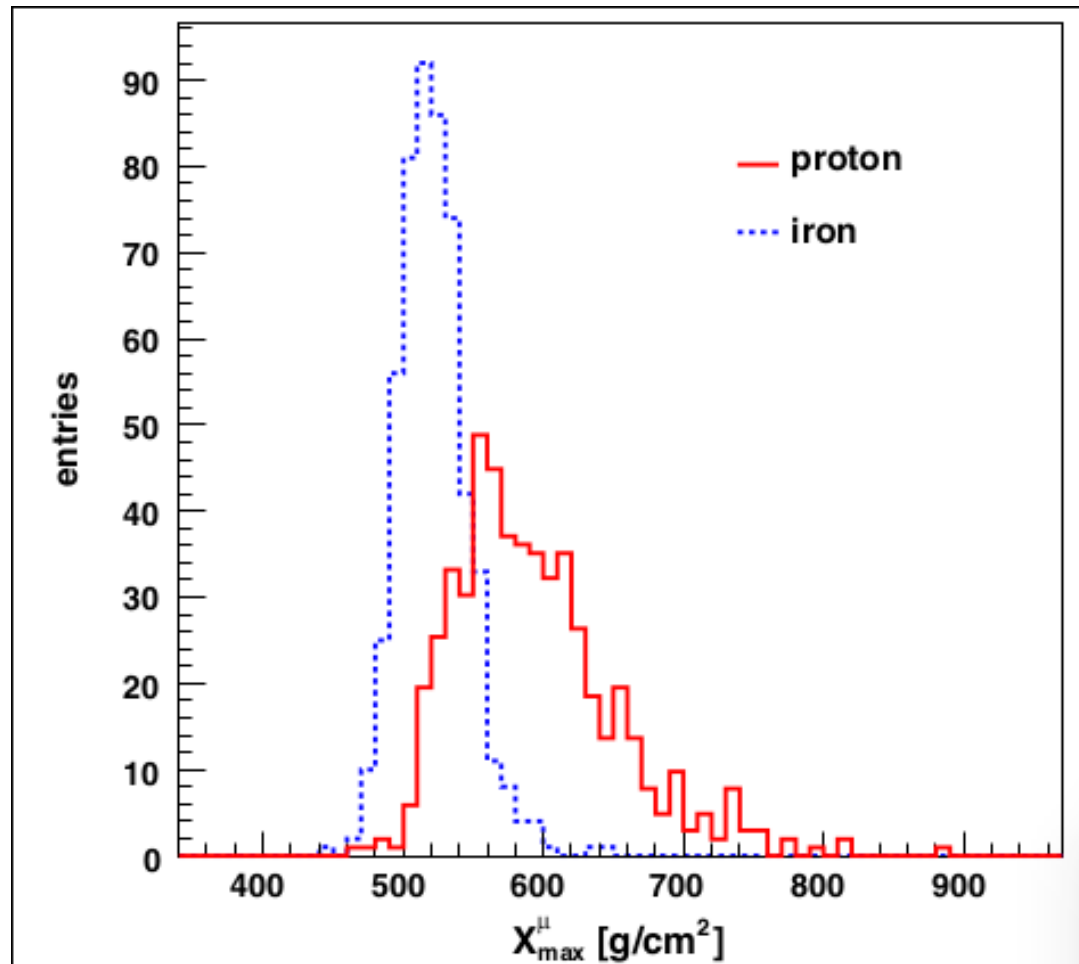


FIG. 4 (color online). X_{\max}^{μ} distributions for proton and iron showers simulated at 30 EeV with EPOS-LHC at zenith angles between 55° and 65° . The mean value and the rms of the distributions show a clear dependence on the mass of the primary cosmic ray. For the construction of the MPDs, only muons reaching the ground at distances greater than 1700 m were considered.